ACS OMEGA

http://pubs.acs.org/journal/acsodf

Article

2D Material-Based Surface-Enhanced Raman Spectroscopy Platforms (Either Alone or in Nanocomposite Form)—From a Chemical Enhancement Perspective

Published as part of ACS Omega special issue "Celebrating 50 Years of Surface Enhanced Spectroscopy".

Dipanwita Majumdar*

Cite This: *ACS Omega* 2024, 9, 40242−40258

Read Online

ABSTRACT: Surface-enhanced Raman spectroscopy (SERS) is a vibrational spectroscopic technique with molecular fingerprinting capability and high sensitivity, even down to the single-molecule level. As it is 50 years since the observation of the phenomenon, it has now become an important task to discuss the challenges in this field and determine the areas of development. Electromagnetic enhancement has a mature theoretical explanation, while a chemical mechanism which involves more complex interactions has been difficult to elucidate until recently. This article focuses on the 2D material-based platforms where chemical enhancement (CE) is a significant contributor to SERS. In the context of a diverse range (transition metal dichalcogenides, MXenes, etc.) and categories (insulating, semiconducting, semimetallic, and metallic) of 2D materials, the review aims to realize the influence of various factors on SERS response such as substrates (layer thickness, structural phase, etc.), analytes (energy levels, molecular orientation, etc.), excitation wavelengths, molecular resonances, charge-transfer transitions, dipole interactions, etc. Some examples of special treatments or approaches have been outlined for overcoming well-known limitations of SERS and include how CE benefits from the defect-induced physicochemical changes to 2D materials mostly via the charge-transport ability or surface interaction efficiency. The review may help readers understand different phenomena involved in CE and broaden the substrate-designing approaches based on a diverse set of 2D materials.

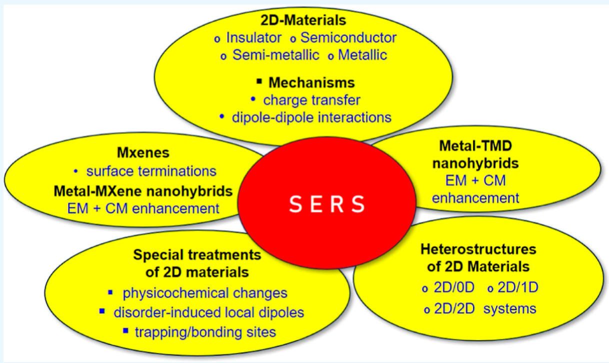

1. INTRODUCTION

Despite the promising combination of the nondestructive nature of the Raman probing technique with the high chemical specificity of investigated samples, the low sensitivity limited the application of Raman spectroscopy until the discovery of surface-enhanced Raman spectroscopy (SERS). The reason is the inherently small Raman scattering cross-section (e.g., 10^{-30} cm^2 per molecule). SERS makes up this deficiency mainly via plasmon-mediated amplification of electrical fields. In 1974, SERS was accidently discovered by Fleischmann and co-workers.[1] During Raman scattering measurements, the authors observed an unexpected signal increase from pyridine adsorbed onto rough silver electrodes and attributed the enhancement to a higher number of adsorbed molecules available for the study due to an increased surface area. This new phenomenon stimulated a great interest (see Figure 1). In 1977, both Jeanmaire and Van Duyne[2] and Albrecht and Creighton[3] independently concluded that the large enhancement observed (around 10^5 to 10^6) could not be simply explained by the increase in the number of scatterers. Since then, SERS has continuously been studied to understand its nature and origin. After a long-run debate, it is now widely accepted that the enhancement in SERS sprouts from two distinct mechanisms, namely, an electromagnetic (EM) enhancement and a chemical enhancement (CE).

The EM mechanism dominantly contributes to SERS. Molecules situated in the immediate or near vicinity of metal nanostructures or metal surfaces with nanoscale roughness experience an enhanced EM field compared to the incident excitation due to localized surface plasmon resonance (LSPR) that lead to orders of magnitude increase in Raman yield[4−7] (see Figure 2). This EM enhancement directly depends on the material and morphology of the substrate, and the enhancement factor (EF) can be as high as 10^8 or more, whereas CE is a short-

Received: July 23, 2024
Revised: August 28, 2024
Accepted: August 30, 2024
Published: September 11, 2024

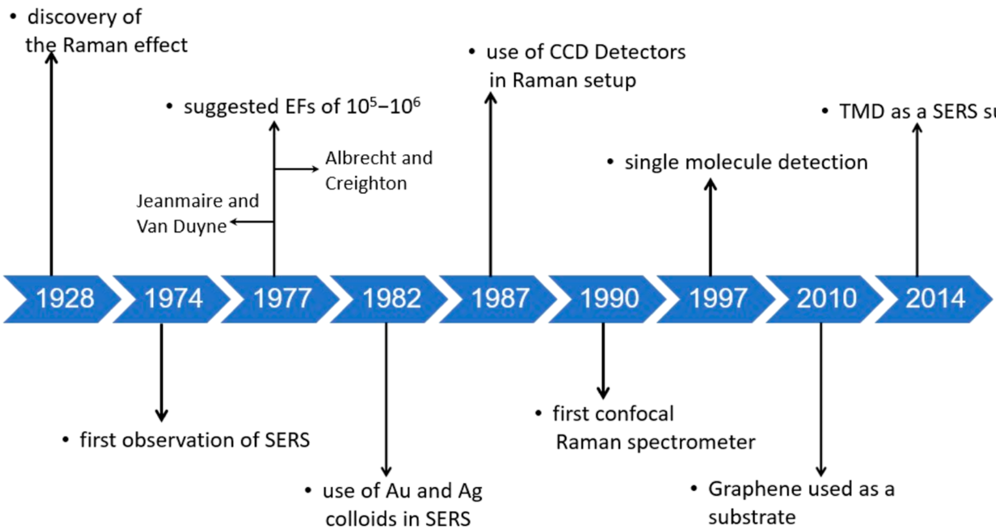

Figure 1. Timeline of the crucial events contributed significantly to the advancement and realization of the SERS technique.

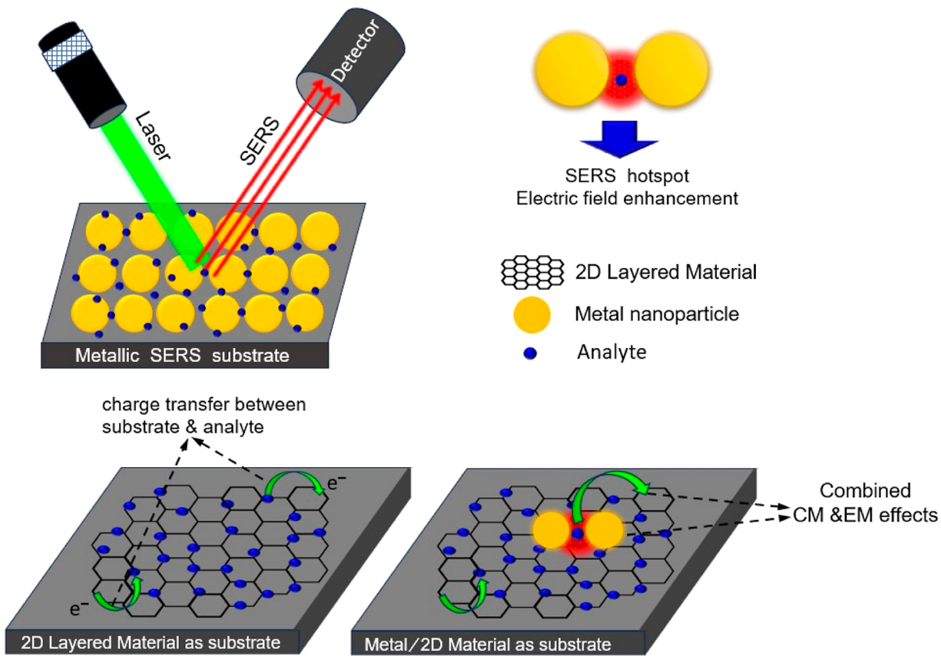

Figure 2. Schematic illustration of the EM and CE mechanism of SERS.

range effect with an EF typically of the order of 10^1 to 10^3 and includes different transitions or processes.[8−10] The CE contribution is usually difficult to assess when it coexists with the EM effect and is often regarded as a secondary factor. The combination of both enhancing pathways gives SERS a significantly improved sensitivity. Au and Ag have negative real dielectric constants and induce strong LSPR in the visible and near-infrared range. Hence, in the last 50 years, great efforts have been made toward an ideal SERS substrate largely focusing on the nanoscale design of Au and Ag using various chemical and physical fabrication methods.[6,7,11−16] With the progress of research in nanotechnology, development of instrumentation, and continuous exploration by researchers, SERS has now matured into a highly sensitive and user-friendly detection technique (Figure 1). It can simultaneously detect a single molecule and provide its chemical fingerprint.[17,18]

Despite many advantages, the routine application of metal SERS substrates has been limited. Size, shape, distribution, and in-between gap of the plasmonic nanostructures are crucial factors in the determination of EF.[19−22] Precise control over nanostructure fabrication is not always easy to attain and often leads to a high variability in EFs. In many synthesis processes, the inevitable introduction of impurities onto the metal surface could also reduce the SERS activity. Although the nanostructured silver surface provides intense SERS signals, the silver surface is not chemically and environmentally stable. Under normal conditions, the poor stability causes deterioration of the enhancing activity over time. Attempts have been made to improve the chemical[23,24] and thermal stability[25,26] though. One unavoidable barrier for Ag- or Au-based substrates is of course the high price of raw materials. The single use of substrates adds to the expense, as well. The clear evidence of graphene's enhancing capacity, owing to its distinct structural and physical/

https://doi.org/10.1021/acsomega.4c06398
ACS Omega 2024, 9, 40242−40258

chemical properties, unfolded a new perspective on SERS.[27−30] Different noncarbon layered materials have also been explored.[31,32] However, the family of transition metal dichalcogenides (TMDs) with diverse categories (insulating, semiconducting, semimetallic, and metallic) introduced unique platforms for extensive studies.[33,34] Though a considerable part of the sensitivity is lost, observing TMD-based SERS (plasmon-free) is also important for the realization of the CE mechanism because of no interference from the EM field enhancement. In the past few years, many strategies have been employed to improve SERS efficiency, including phase transition, doping, plasma treatment, etc.[35−37] Various nanohybrid systems of noble metals and different 2D materials such as graphene,[38−42] graphitic carbon nitride (g-C_3N_4),[43,44] hexagonal boron nitride (h-BN),[45−47] black phosphorus,[48,49] and TMDs[50−53] also have been found effective in enhancing signals which are based on the combined chemical mechanism (CM) and EM effects from the 2D materials and metal nanostructures, respectively (Figure 2). The SERS research has seen rapid growth in this field. In the past decade, the family of 2D materials has further been extended by the carbides, nitrides, or carbonitrides of transition metals known as MXenes, which are now gaining popularity in SERS studies. Surface terminations of MXenes introduce additional functional properties. The wide research, therefore, makes SERS a thriving technique covering fundamental and diverse fields of applications across physics, chemistry, and biology including biosample analysis,[54−56] microbiology,[57] food safety,[58,59] toxicology,[60] narcotics,[61] forensic science,[62] biomedical fields, e.g., clinical diagnosis and therapeutic aspects,[63−67] and so forth.

The EM mechanism has a mature theoretical explanation[68,69] and there are also excellent review articles on the fundamentals of the effect.[70−72] EM-based substrates have also been reviewed many times with a focus on synthesis methods. This review largely focuses on the 2D material-based SERS platforms with an emphasis on the CE contribution to SERS. The article aims to realize how various factors such as substrates (layer thickness, structural phase, etc.), analytes (energy levels, molecular orientation, etc.), excitation wavelengths, molecular resonances, charge-transfer (CT) transitions, dipole interactions, etc. influence SERS response. A section includes some potential defect engineering strategies placed by researchers and discusses how the consequent alteration in the density of states (DOS) or creation of surface active sites could directly influence the SERS effect via improved charge-transport ability or surface interaction efficiency. The review may help readers understand the different origins and processes behind CE and figure out exciting substrate-designing approaches based on a diverse set of 2D materials.

2. CHALLENGES WITH NOBLE-METAL-BASED SERS SUBSTRATES

Hotspots are locations in the vicinity of the plasmonic nanostructures where the local field is enhanced tremendously depending on the collective oscillations of free electrons when the nanostructures are irradiated by an external EM field with a certain frequency.[73] The frequency of electron oscillations depends on the density of electrons, the effective electron mass, and the shape and size of the charge distribution.[74] If the frequency of the incoming radiation is resonant with that of the electron oscillation, then the excitation process is termed surface plasmon resonance (SPR). The signal strength of a probe molecule crucially depends on its location within the plasmonic structures, more specifically, on the nanoscale distance from the hotspots; even a minor change can lead to a significant difference.[23] The randomly oriented or aggregated nanostructures thus often cause a high degree of variability in the EFs that leads to a lack of uniformity and reproducibility in the SERS results. Lithography-based methods, including optical, electron-beam, and soft lithography, have good control over the shapes of metal nanostructures and the distance between them[75−77] and can efficiently fabricate highly ordered SERS substrates. However, the main drawback is the time-consuming process with multistep protocols, which makes mass production difficult. Colloidal metal nanoparticles (NPs) make popular choices as SERS substrates due to relatively inexpensive and simple techniques used in fabrication, such as easy chemical reduction of Ag, Au, and Cu salt solutions.[78,79] In many synthesis methods, the inevitable introduction of impurities on the metal surface could also reduce the SERS response. While the use of different metals including copper (Cu),[80] aluminum (Al),[81] platinum (Pt),[82] palladium (Pd),[83] iron,[84] etc. has been reported in SERS studies, Au and Ag, however, are most widely adopted due to their optical absorptions in the visible region and strong plasmonic effect.[85−87] Studies have found the SERS response to be highly sensitive to the shapes of the nanostructures. NPs with anisotropic morphologies such as nanocubes,[88] nanorods (NRs),[89] nanostars,[90] nanoflowers,[91] nanoneedles,[61] etc. exhibit high field enhancement. Taylor et al. though reported the photothermal reshaping behavior (instability) of gold NRs irradiated with fs laser pulses.[92] The surface diffusion model indicated that nanostructures with larger aspect ratios are more prone to induce reshaping, as the surface atoms are much easier to diffuse around. Therefore, applications with anisotropic NPs having sharp geometric features need to be considered for surface diffusion-driven shape changes. Besides monometallic substrates, bimetallic substrates, for example, Au@Ag NR dimers,[93] concave Au/Pd nanocrystals,[94] Au@Ag/3D-Si,[95] DNA-mediated Au−Ag nanomushrooms,[96] Au−Ag/Au core/shell NPs,[97] Ag−Au−PVA thin film,[98] etc., have been fabricated as well. Here, it is noteworthy that to attain optimum sensitivity and precision, substrates are usually used for a single time, which makes SERS a costly technique. Moreover, silver with the best enhancement efficiency is easily affected by the environment. For sustained performance, strict storage conditions are required. In metal-based substrates, CE usually occurs alongside the EM effect, and due to the difficulty of separating and quantifying the effect experimentally, CE was less studied in the early studies. It is worthwhile to note that compared to the normal Raman signal (i.e., at non-SERS conditions), the SERS spectrum of probe molecules sometimes exhibits specific spectral changes such as peak shifts, change in intensity ratios, or even the appearance of new modes that the EM theory does not account for. 2D materials introduce a new perspective to the SERS study where CE is often proposed as the main enhancement mechanism and can be studied extensively. We will, however, gradually see (in the following sections) that CE does not refer to a specific phenomenon/route but it has a "comprehensive" interpretation uniting several different backgrounds and processes.

In the post-graphene era, TMDs have been significantly explored in SERS. TMDs are layered materials and generally adopt the formula MX_2, where M is a group IV (for example, Ti or Zr), group V (for example, V, Nb, or Ta), or group VI (for example, Mo or W) transition metal element and X is a chalcogen from group 16 (for example, S, Se, or Te). A plane of

https://doi.org/10.1021/acsomega.4c06398
ACS Omega 2024, 9, 40242−40258

transition metal atoms is sandwiched between two planes of chalcogen atoms. The structure and morphology of TMDs are usually similar to those of graphitic structures. Some representative examples of this class of materials are MoS_2, WS_2, WSe_2, and $MoSe_2$. Analogous to graphene, they have strong intralayer covalent bonding and display weak van der Waals (vdW) interactions between the adjacent layers; but in contrast, they have unique physicochemical features, including layer-number-dependent band gap structures, ranging from 1 to 2 eV.[99−103]

2D materials with large flat surfaces not only facilitate a higher uniform Raman signal across the whole surface but also offer better chemical stability essential for practical use. Besides, the low cost of raw materials (due to abundant availability) combined with the ease of preparation by exfoliation or chemical techniques justifies further SERS studies on 2D layered materials despite their moderate EF. A SERS spectrum consists of the signals coming from the analyte and occasionally from the substrate; however, sometimes the background noises are also attached to the spectrum which could originate from photoluminescence and fluorescence and/or Raman signals of the solvent, reagent byproducts, or impurities. Therefore, at extremely low analyte concentrations or when the analyte signal is itself weak, there is a strong possibility that noises mask the analyte data in the SERS spectrum. Like graphene, different TMD materials possess a promising fluorescent quenching efficiency that facilitates the detection of some aromatic molecules. The following sections provide an overview of the significant aspects of 2D material-based SERS platforms.

3. RESULTS AND DISCUSSION

3.1. 2D Materials Alone. Some recent papers are discussed in this section that cover a diverse range and categories of 2D materials (insulating, semiconducting, semimetallic, and metallic) and help understand the CE mechanism and its contribution to SERS.

SERS activity on a molybdenum disulfide (MoS_2) substrate was first reported by Ling et al.[33] Using a copper phthalocyanine (CuPc) molecule as a probe, the authors compared the SERS performances of graphene and h-BN with MoS_2 and explained the different EFs from the different 2D materials based on their distinct electronic and chemical properties (Figure 3A). For graphene, the EM mechanism is negligible as graphene's SPR lies in the terahertz region and the experiment was carried out with a 633 nm laser excitation wavelength; second, because of nonpolar bonds, the dipole−dipole interaction between graphene and CuPc is insignificant as well. On the other hand, h-BN with a similar hexagonal structure has a wide band gap (insulating) and high polarity. Therefore, instead of the efficient CT mechanism in zero-gap graphene, h-BN induces a strong interface dipole−dipole interaction with the CuPc molecule which drives the enhancement. As the dipole mechanism is a single-layer effect, the CE is independent of h-BN's thickness (Figure 3B,C), which is distinct from the results on graphene. However, for MoS_2, a semiconductor, the enhancement mechanism is different. Each layer of MoS_2 is composed of S−Mo−S stacks and has a covalent Mo−S bond with polarity in the vertical direction to the surface and offers the potential for a dipole-driven enhancement. Therefore, both CT and dipole−dipole coupling may coexist in MoS_2 and contribute to signal enhancement. Muehlethaler et al. reported an enhancement (>3 × 10^5) in the SERS signal from an organic molecule (4-mercaptopyridine, 4-MPy) when placed in the near field of a

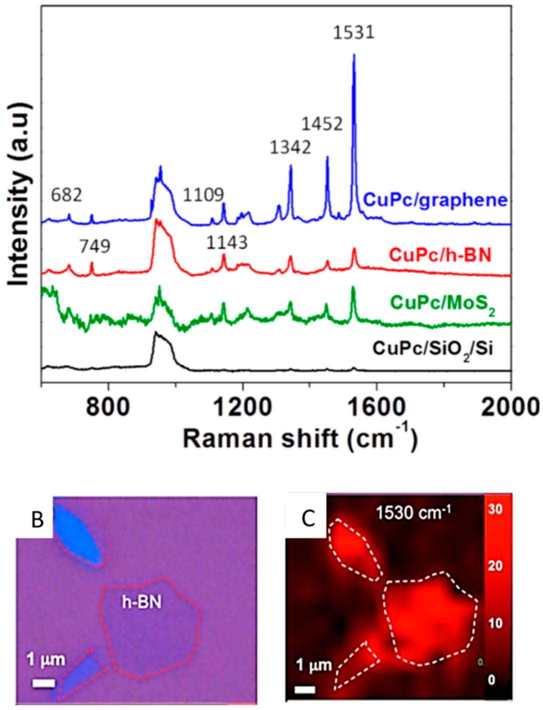

Figure 3. (A) Raman spectra of the CuPc (2 Å) molecule on the blank SiO_2/Si substrate (black line), graphene (blue line), h-BN (red line), and MoS_2 (green line) substrates. The numbers marked on the peaks are the peak frequencies of the Raman signals from the CuPc molecule. For all of the spectra, the baseline correction was removed to have a better comparison. (B) Optical image of a h-BN flake. Some h-BN flakes are marked by arrows or by a red dashed ring. (C) Raman mapping image for the CuPc vibrational mode at 1531 cm^{-1} corresponding to (B). Reprinted with permission from ref 33. Copyright 2014 American Chemical Society.

MoS_2 monolayer. At the interface of the 2D semiconductor and organic molecule, a CT state formed which promotes the enhancement when in resonance with the laser excitation source (488 nm).[104] The EF was calculated using the equation

$$EF = \frac{I_{surf} \times N_{bulk}}{I_{bulk} \times N_{surf}}$$

N_{bulk} is the number of molecules sampled for the bulk 4-MPy, N_{surf} is the number of molecules on the MoS_2 contributing to the enhancement, and I is the corresponding intensity of the line chosen (C−H bending line at 1280 cm^{-1}).

The atomically flat surfaces of 2D materials allow target molecules to be in close contact with the underlying substrate, and the enhancement is mainly found to depend on the amount of CT between them. The thickness dependence of the CE effect was similar for MoS_2 and graphene where a single-layer system provided a maximum EF, but it was distinct for the WSe_2 substrate, in which a high CE effect was preserved until two layers.[105] In another study, Meng et al.[106] examined the crucial role of layer numbers in obtaining improved CT on a layer-controllable WS_2 film synthesized via the CVD method. Though EFs were not calculated, monolayer WS_2 exhibited the strongest Raman signal toward the R6G probe. From monolayer to few-layer, the band structure WS_2 translates from direct to indirect band gap.[107] The indirect relaxation process makes electrons stay for a longer time in the few-layer WS_2 than in the single-layer one, which inevitably reduces the CT yield, and the

https://doi.org/10.1021/acsomega.4c06398
ACS Omega 2024, 9, 40242−40258

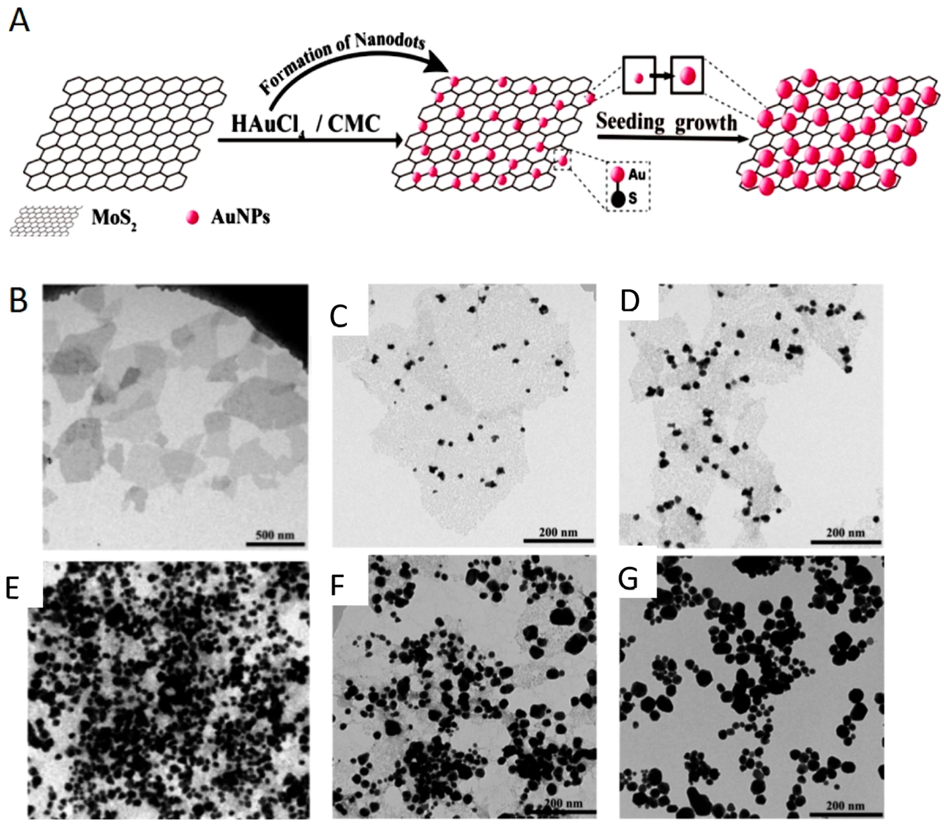

Figure 4. (A) Schematic illustration of synthesizing the AuNPs@MoS_2 nanocomposite. TEM images of (B) MoS_2 and (C−G) AuNPs@MoS_2 nanocomposites. Reprinted with permission from ref 120. Copyright 2014 American Chemical Society.

enhancement gradually decreases with the increase in the layer number.

3.1.1. Impact of Molecular Orientation. Employing a planar molecule (CuPc) as a probe, Ling et al. observed that CE is highly sensitive to its molecular orientation.[108a] On top of graphene (mechanically exfoliated), the orientation of the CuPc molecule in a Langmuir−Blodgett (LB) film was changed from an upstanding to a lying-down state via annealing at an appropriate temperature (of 300 °C). Compared to the Raman spectra of the as-prepared CuPc LB film (upstanding state), a higher enhancement was recorded in a planar orientation of the same due to stronger $\pi-\pi$ interactions between CuPc and graphene. Yang et al. studied the SERS effect on three single-layer surfaces, namely, graphene oxide (GO), reduced graphene oxide (r-GO), and graphene (SLG), using R6G as a probe and observed substrate-selective enhancement of R6G vibration modes.[108b] One characteristic mode of R6G observed at around 1648 cm^{-1} is assigned to an aromatic stretching vibration mode. On GO, for example, the intensity of this peak was much lower than the other characteristic modes, whereas on SLG, the same mode at 1648 cm^{-1} attained the highest intensity, suggesting strong interaction of R6G molecules with SLG through the aromatic rings. Differences in the bonding and orientation of adsorbed R6G on these substrates due to the different local chemical groups could be the possible reason behind the significant spectral differences.

3.1.2. Photostability of the Probes. The assessment of the SERS effect is intimately tied to the stability of the probes during the measurements.[109] The photostability of the probes depends on the conditions under which the experiment is carried out. For example, fluorescent dyes can degrade upon intense light exposure. Studies reported that being on top of the organic molecules, graphene could act as a good barrier film for oxygen and greatly enhance the photostability of the probe.[110,111] In another study, Qiu et al. observed a prominent suppression of photobleaching and fluorescence of the tested molecules from a SERS substrate prepared by synthesizing a few layers of MoS_2 directly on a pyramid-Si platform.[112]

3.1.3. Structural Phase and DOS. Density functional theory suggested a strong correlation between the SERS performance and DOS near the Fermi level.[113] In 2H-MoS_2 material, the photoinduced CT (PICT) between the analytes and MoS_2 is mainly responsible for the enhancement and involves a two-step process, for example, (i) electrons are excited from the highest occupied molecular orbital (HOMO) into the lowest unoccupied molecular orbital (LUMO) of the dye, leaving holes in the HOMO level, and subsequently, (ii) electrons migrate from the valence band (VB) edge of the MoS_2 material into the HOMO, thus recombining with the holes. It is, however, noteworthy that monolayer 1T-MoS_2 is metallic in nature. With 1T-MoX_2 monolayers as SERS substrates, Yin et al.[36] observed a significant increase in Raman intensity for the probe molecules tested. The authors argued that electron transfer from the Fermi energy level of metallic 1T-MoX_2 to the HOMO level of the probe molecules is more efficient than the process from the top of the VB of semiconducting 2H-MoX_2.

Song et al. reported the SERS performance of as-obtained metallic 2D niobium disulfide (NbS_2) which shows an impressive detection limit down to 10^{-14} mol·L^{-1}.[113] Compared to graphene, 1T-MoS_2, and 2H-MoS_2, NbS_2 featured abundant DOS that increases the intermolecular CT probability and induces prominent Raman enhancement. It is noteworthy that

https://doi.org/10.1021/acsomega.4c06398
ACS Omega 2024, 9, 40242−40258

even if most 2D materials are found to have the best SERS performance in monolayer samples, certain 2D materials can have superior Raman enhancement in thicker samples though. Platinum telluride ($PtTe_2$), a kind of type-II Dirac semimetal, revealed such a unique thickness-dependent SERS effect with a four-layered (4L-$PtTe_2$) sample exhibiting the strongest Raman intensity toward R6G which is attributed to its high DOS near the Fermi level and strongest built-in electric field at the interface of molecule/$PtTe_2$ compared with the case of $PtTe_2$ with other layer numbers.[114] SERS performance of another semimetallic material $MoTe_2$ was presented by Fraser et al.[115] A few-layer thick film detected clinically relevant molecules (β-sitosterol) down to the nanomolar level. The difference between HOMO (−6.16 eV) and LUMO (0.77 eV) levels in β-sitosterol significantly exceeds the excitation wavelengths [785 nm (1.53 eV) or 532 nm (2.3 eV)]. Hence, the sensing was realized via nonresonant chemical interactions between the surface and the adsorbate at the ground state.

SERS response has also been observed in other TMDs. For example, ReS_2, which, unlike common MX_2 (M = Mo or W and X = S or Se), has a naturally distorted 1T′ crystal structure with low lattice symmetry. The unique anisotropic (electrical and optical) properties and weak interlayer interactions of ReS_2 provide a broad application prospect including SERS.[116] Zhang et al. studied the controllable growth of single-crystal 2D ReS_2 flakes with layer numbers from 1 to 18.[117] Studies reported a layer-number-dependent SERS response of ReS_2.[116,117] Wang et al. examined the significance of the underlying substrate of ReS_2 in fluorescent background suppression of SERS signals and reported a robust enhancing performance of large-area monolayer ReS_2/mica films; however, the LOD (∼10^{-7} M for R6G) was far less than that of noble-metal-based substrates and thus limits its trace detection capability.[118] Plasmon-free SERS has been studied on 1T′-W(Mo)Te_2 as well.[119] Strong interaction between the analyte and 1T′-W(Mo)Te_2 and the abundant DOS near the Fermi level of the semimetal 1T′-W(Mo)Te_2 collectively promoted CT resonance in the analyte−telluride complex, leading to sensitivity down to the femtomolar level for R6G, the same order of magnitude as in noble metals.

3.2. Metal−2D Material Nanohybrids. The beginning of this section focuses on the various kinds of methods that are employed to grow NPs on the TMD surfaces. For example, Su and co-workers[120] fabricated AuNPs@MoS_2 SERS substrates with $HAuCl_4$ as a precursor (microwave-assisted hydrothermal method). MoS_2/AuCl4$^-$ formed a redox pair, that allowed spontaneous reduction of gold ions to gold NPs (Figure 4A). The density of the AuNPs on the MoS_2 surface (Figure 4B) could be controlled by the concentration of $HAuCl_4$. The substrates having AuNPs close to each other and with a little aggregation (Figure 4E) exhibited higher SERS activity in detecting R6G compared to other AuNPs@MoS_2 substrates with either damaged or disappeared MoS_2 nanosheets (Figure 4C,D,F,G). The synergetic contribution of plasmons and CT was attributed to the amplified SERS activity. Daeneke et al. reported that the morphologies of metal Ag (NPs, nanoplatelets, nanobranches, etc.) integrated into the MoS_2 surface, via photoexcitation in the presence of Ag ions, largely depend on the illumination time.[121] Under laser irradiation, electrons of the semiconductor TMD (MoS_2) can be excited from the VB to the conduction band (CB), yielding electron−hole pairs. Now depending on the redox potential of metal ions and the band gap of the semiconductor, CT can occur between them that may lead to an effective metal-ion reduction followed by in situ metal deposition forming metal−TMD nanohybrids.[122] Laser-modified TMD surfaces are also found to facilitate the metal-ion reduction process. Lu et al. employed a tightly focused laser beam to premodify the MoS_2 film to achieve active surface domains and when immersed in $AuCl_3$ solution, the pruned area with partially unbound sulfur attracts the Au^{3+} precursor at the initial stage and acts as the first nucleation center for the Au particle growth. A variation in the laser power and the reaction time in the $AuCl_3$ solution determines the distribution and size of the AuNPs.[123] An advantage of this approach is that without using any masks, a SERS platform was realized with a micropatterned MoS_2 film containing metal NPs of controlled size and density. Later, in another study, Zuo et al.[124] used temporally shaped fs laser pulses to develop Au−MoS_2 hybrid structures by simultaneously tuning the chemical and physical properties of MoS_2, where the edge-active sites with unbound sulfurs and the surface periodic structures drive the reduction of gold NPs, and assist the shape-controllable growth of AuNPs on MoS_2 surfaces, respectively.

In search of a promising enhancing platform, various substrates with different arrangements, shapes, or morphologies have been tested, for example, (i) spherical MoS_2 nano-objects decorated with Au NPs,[125] (ii) MoS_2 nanoplates functionalized with AgNPs,[126] (iii) MoS_2 nanodonuts grown on graphene,[127] etc. Few studies reported designs of SERS platforms using TMDs other than MoS_2; for instance, AuNPs on the surfaces of WS_2,[52,128] WSe_2,[53,129] and $MoSe_2$.[130] In a recent report, authors suggested that porous structures of ReS_2 nanoflowers can effectively confine the growth of AuNPs, leading to a ReS_2/AuNPs composite structure that detected pesticides at 10^{-10} M, originating from a synergistic (CM and EM) enhancement effect.[131] Jung et al. prepared a sponge-based SERS sensor formed of silver nanowires coated with hydrophobic h-BN for the simultaneous separation and detection of organic pollutants.[132]

In another example, Jiang and co-workers[133] prepared a platform exploiting the collective ability of MoS_2, Ag NPs, and treated silicon substrate pyramidal Si (PSi) and reported its superior performance compared to the AgNPs@PSi and the MoS_2@AgNPs@flat-Si substrates. The MoS_2 film isolates the AgNPs from the outside environment and protects them from oxidation. Toward SERS, each component of the substrate contributed: MoS_2 owing to the efficient adsorption of target molecules and CE; EM effect from AgNPs; and the relatively larger scattering cross-section from PSi. The minimum detected R6G concentration from the MoS_2@AgNPs@PSi substrate was 10^{-11} M. Tegegne et al.[134] demonstrated the SERS response of Ag nanocube-decorated 1T-MoS_2 nanosheets fabricated on a flexible filter paper. The substrate exhibits a good EF and a low detection limit (LOD) of 10^{-12} M, for R6G. The 1T-MoS_2 nanosheets form a scaffold that physically holds the Ag nanocubes. Moreover, the porous structure of the filter paper improved the assemblage of the substrate to get a high hotspot density. The notable SERS activity was attributed to the synergistic effect of (i) the EM enhancement generated from the nanogaps of the plasmonic Ag nanocubes and (ii) the dipole−dipole coupling and CT between the 1T-MoS_2 nanosheets and the detected molecules. For achieving effective CT, the purity of the 1T-phase MoS_2 material is crucial. However, stability issues hinder the synthesis of metallic 1T-MoS_2 by any simple approach.

https://doi.org/10.1021/acsomega.4c06398
ACS Omega 2024, 9, 40242−40258

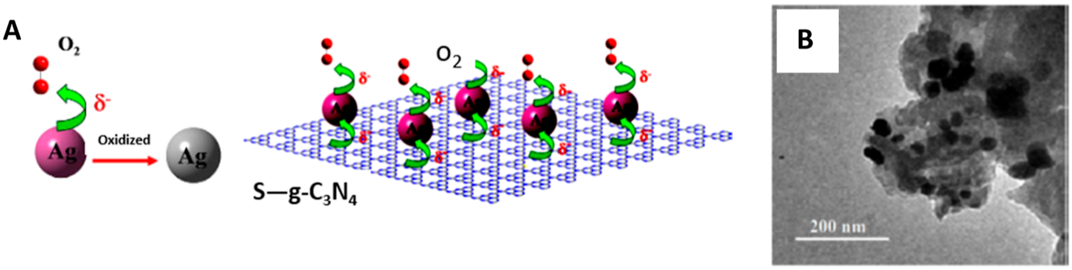

Figure 5. (A) Schematic illustration of the CT process among S-*g*-C_3N_4, O_2, and Ag. The label *δ* denotes the negative charge of the Ag surface or S-*g*-C_3N_4. (B) TEM image of the S-*g*-C_3N_4/Ag hybrid. (A,B) Reprinted with permission from ref 43. Copyright 2016 the author(s).

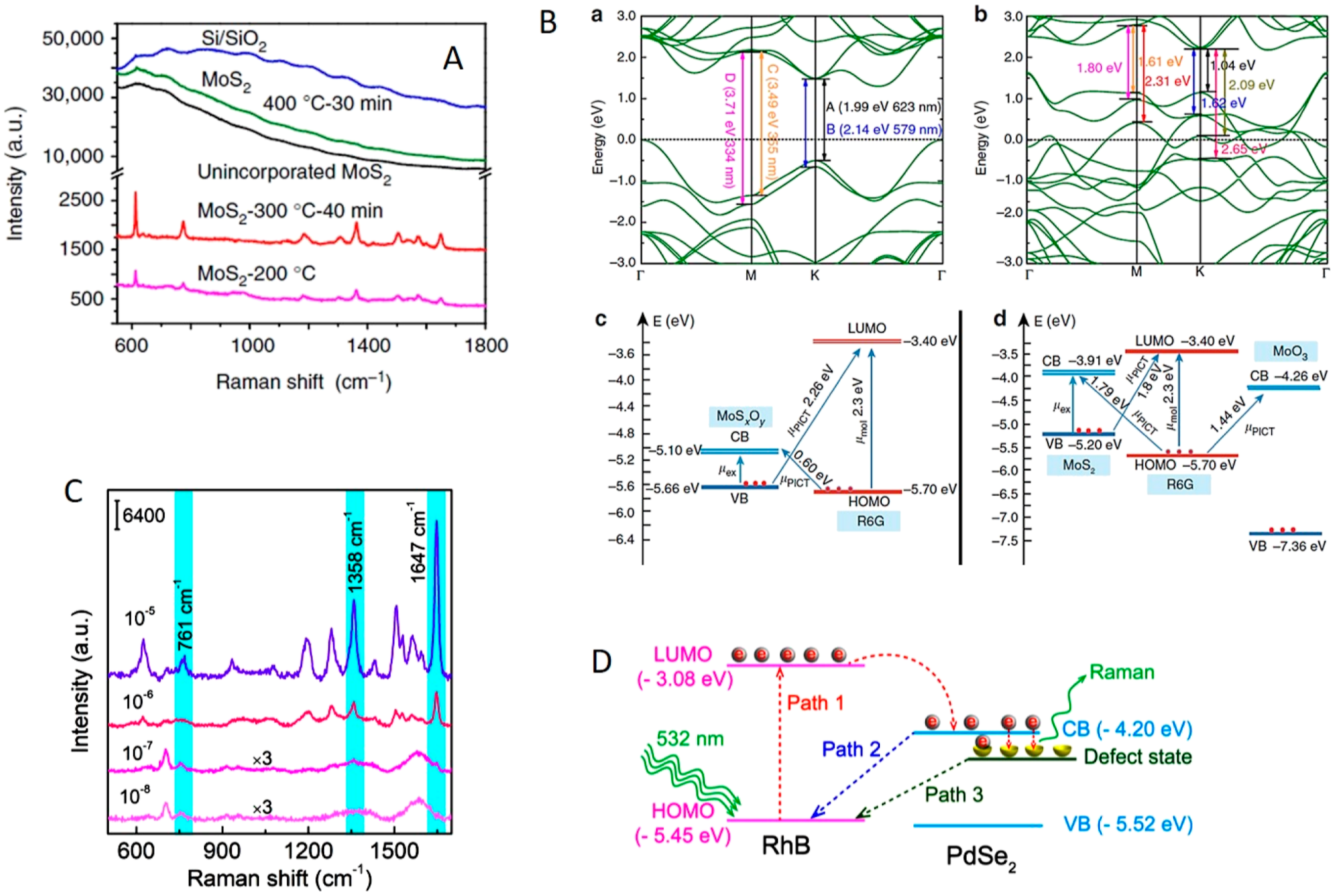

Figure 6. (A) Raman profile of R6G (10^{-6} M) on substrates deposited with an unincorporated MoS_2 sample, hydrothermally treated oxygen-substituted MoS_2 sample at 200 °C, partially oxidized sample at 300 °C for 40 min, completely oxidized MoO_3 sample, and bare SiO_2/Si. (B) Energy-level diagrams illustrating the electronic transitions. The calculated band structures of MoS_2 (a) and MoS_xO_y (b) taking the Fermi level as a reference. Schematic energy-level diagrams of R6G on (c) MoS_xO_y and (d) MoS_2 and MoO_3 with respect to the vacuum level. (C) Raman spectra of 10^{-5}, 10^{-6}, 10^{-7}, and 10^{-8} M RhB on $PdSe_2$. (D) Energy band diagram showing the CT pathways in the RhB/$PdSe_2$ hybrid system. (A,B) Reprinted with permission from ref 138. Copyright 2017 the author(s). (C,D) Reprinted with permission from ref 141. Copyright 2023 the author(s).

3.2.1. Attempts toward Chemical Stability. Ag is known to deliver excellent SERS performance but has a major weakness in oxidation in air. This part of the section focuses on some attempts made toward the chemical stability of Ag-based substrates. A honeycomb lattice of graphene could prevent the penetration of small molecules like hydrogen and water[135] and could endow SERS platforms with potential sustainability. Suzuki and Yoshimura[136] fabricated a graphene-coated silver SERS substrate that showed high tolerance in concentrated hydrochloric acid (35−37%) and heated air up to 400 °C. A study by Chen et al. reported good stability and a long lifetime of a MoS_2/AgNPs hybrid system which was designed by synthesizing a few layers of MoS_2 directly on Ag NPs via the thermal decomposition method.[137] A comparative study of SERS activity between the AgNP system and MoS_2/AgNPs hybrid system over a given period displayed a lower degree of decay (dropped by 20%) in the SERS results for the hybrid system and a rapid deterioration in the Raman activity for AgNPs (dropped by 45%) caused by oxidation. Hybrid substrates of graphitic carbon nitride (g-C_3N_4) and AgNPs have shown prominent stability due to strong interaction and the CT effect between them (Figure 5A,B). The net positive surface charges on the Ag atoms in g-C_3N_4/Ag substrates suggested that these Ag atoms are difficult to oxidize.[43] On the other hand, h-

https://doi.org/10.1021/acsomega.4c06398
ACS Omega 2024, 9, 40242−40258

BN has exceptional chemical and thermal stability, suggesting that exposed h-BN will hold its atomic structure in gas or liquid environments for an extended duration even at elevated temperatures. Chugh et al. applied atomically thin h-BN layers for passivating gold and silver NPs and demonstrated the effectiveness of h-BN in retaining the SERS activity of h-BN-shielded Ag NPs even at high temperatures.[31]

3.3. Special Treatments of 2D Materials toward SERS. This section will outline some special treatments and potential defect engineering strategies in 2D materials toward the development of effective SERS substrates.

3.3.1. Impact of Defects and Doping. Using MoS_2 as a model material, Zheng et al.[138] put forward a general oxygen incorporation-assisted strategy that is very effective in improving the semiconductor substrate−analyte molecule interaction. Compared with unincorporated, oxygen-substituted, and completely oxidized MoS_2 (identified as MoO_3), a partially oxidized MoS_2 sample prepared by careful annealing in an air atmosphere not only increases the SERS activity but also suppresses the fluorescence background (Figure 6A). Oxygen incorporation can cause lattice distortion of different degrees in the MoS_2 hosts, where the electronic properties may be significantly altered. Consequent CT efficiency and resulting magnified molecular polarization ultimately impact the enhancement. The authors demonstrated the universality of this strategy by studying other TMDs, including WS_2, WSe_2, and $MoSe_2$. Zuo et al. studied the impact of S vacancies in MoS_2[139] on SERS via femtosecond pulse laser treatment. The authors argued that induced defect/active sites, including micro- or nanoscale fractures and S atomic vacancies, were responsible for the enhanced SERS activity. Later, with diclofenac (an antibiotic contaminant) as a model probe, Quan et al.[140] reported its accurate observation at a nanomolar concentration level using MoS_2 with S vacancies as a SERS substrate. Both the abundant adsorption sites on the MoS_2 surface (external effect) and altered band structure (internal effect) promote the high SERS activity. Jena et al.[141] examined how defects, nanopores, and edge geometry could impact the SERS performance of Se vacancy-rich dendritic $PdSe_2$ (Figure 6C,D). Multiple CT processes (including defect state-mediated CT mechanism) combined with metal-like behavior (nonplasmonic hotspots) of the dendritic $PdSe_2$ are accountable for the high SERS activity. Co-modified MoS_2 by Ni and O was reported to enhance the polarity and carrier concentration of MoS_2 which leads to a SERS effect comparable to that of noble metals.[142] During annealing, the introduction of the O atoms into the S defects reduces the internal defects of doped MoS_2, improves carrier mobility, and promotes the efficient CT effect of MoS_2. Rare earth dopants have also been explored for enhanced SERS activity. For example, Nd-incorporated MoS_2 improved the enhancement ability based on the energy-level transition and CT effect.[143] The heteroatom doping of WSe_2 with Re and Nb atoms (1T″ Nb, Re-WSe_2) enabled femtomolar-level sensing with long-term stability via electronic structure modulation.[35] Going a step forward, Koklioti et al. tested N-doped and AgNP-decorated TMDs (N-MoS_2/AgNPs) as SERS substrates where CT between the target molecules and modified TMDs, dipole−dipole coupling interactions, and EM fields around AgNPs synergistically led to the enhanced Raman signal.[144] The effect of doping has also been studied for various other layered TMDs to develop practical LSPR-free SERS platforms, such as (i) $SnSe_2$ (doped with sulfur),[145] (ii) 1T′ $ReSe_2$ (doped with vanadium),[146] etc.

An increase in the DOS can be achieved by tuning the atomic ratio of TMDs. In a study, Liu et al.[147] reported how a reduced atomic ratio (Se/W) of 1.96 can increase the exciton and CT resonances in the CuPc−WSe_2 system, which can be correlated to the enhanced SERS performance. The interlayer distance of the TMD material is also found to influence SERS detection ability. Li et al. achieved an EF of the order of 10^5 with a smaller interlayer spacing of MoS_2.[148]

3.3.2. Surface Treatments. Using plasma-processed MoS_2 nanoflakes as a SERS substrate,[149] Sun et al. observed an enhancement in the R6G signal and identified (i) the structural disorder-induced generation of local dipoles and (ii) adsorption of oxygen on the plasma-treated MoS_2 nanosheets as the two important driving forces behind the enhancement. MoS_2-based SERS substrates are most often associated with either monolayers or few layers, which are generally prepared by delicate, complex, and time-consuming synthesis processes that hinder large-scale production and routine use of the SERS technique. To combat this, one-step fs laser pulse treatment[150] and thermal treatment[37] were proposed for bulk MoS_2 to modify the surface. The CM effect benefits from the increase in the direct contact area between the surface and the analytes. Pan et al.[150] observed a high sensitivity for laser-treated MoS_2 where an intense laser pulse was used to heat the pristine bulk MoS_2 surface to a high temperature which caused surface damage and numerous defects. The surface morphology (roughness) changed dramatically with the laser fluence. The improved SERS activity (EF of 1.67×10^5 and sensitivity down to 10^{-8} M for R6G) was ascribed to the surface defects, which can break the original symmetry of R6G to create local dipoles on the surface and result in enhanced CT between MoS_2 and R6G molecules. A major advantage here is that the method does not require additional substrate preparation. Thus, the SERS effect directly benefits from the defect-induced physicochemical changes to 2D materials via charge-transport ability or surface interaction efficiency.

3.4. Homo- or Mixed-Dimensional Composites of 2D Materials in SERS. In recent years, researchers have taken notable approaches to develop homo- or mixed-dimensional composites of 2D materials for the achievement of noble-metal-comparable SERS detection. Ma et al. studied the geometric and electronic structures of graphene adsorption on a MoS_2 monolayer by using density functional theory. Based on calculations, the authors suggested that graphene could bond to MoS_2 through a weak interaction.[151] Later, Ghopry et al. developed a vdW heterostructure by synthesizing TMD (MoS_2 and WS_2) nanodomes on graphene, which exhibited sensitivity in the range of 10^{-11} to 10^{-12} M for R6G. The authors argued that CE cannot be solely responsible for such a high performance mainly based on two observations: first, the enhancement significantly dropped when the nanodomes were replaced by a continuous TMD layer on graphene; second, as compared to graphene only, its Raman signature peak was enhanced significantly while with TMD nanodomes. Hence, the authors attributed the high sensitivity to both CM and EM effects, originating from the dipole−dipole interaction at the TMD/graphene vdW interface and the LSPR effect on the TMD nanodomes/graphene, respectively.[152] Tan et al.[153] observed the Raman enhancement effect on 2D heterostructures formed by stacking a WSe_2 (W) monolayer and graphene (G) together in different orders, including G/W, W/G, G/W/G/W, and W/G/G/W. The G/W and G/W/G/W hybrids exhibit high SERS sensitivity, while W/G and W/G/G/W substrates show

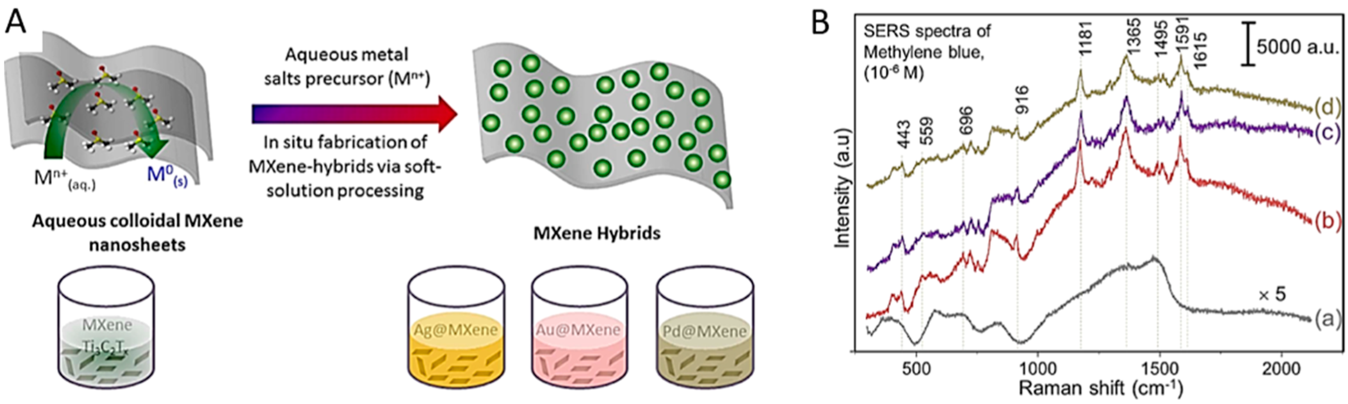

Figure 7. (A) Graphical representation of in situ one-step solution processing synthesis of Ag, Au, and Pd@MXene ($Ti_3C_2T_x$) hybrids by soft-solution processing via a sonochemical approach. (B) Raman spectrum of $Ti_3C_2T_x$ after soaking in MB dispersed in ethanol and subsequent drying. SERS spectra of MB with (b) Ag@, (c) Au@, and (d) Pd@MXene. Reprinted with permission from ref 169. Copyright 2016 the author(s).

intermediate SERS activities between the individual WSe_2 and graphene monolayer. The observations indicated an enhancement effect that is highly dependent on the topmost material of the stacking and varies with the different interlayer couplings within the heterostructures. Wu et al.[154] explored the enhancing ability of MoS_2 quantum dot/r-GO (MoS_2 QD/rGO) nanocomposites (LOD of 1×10^{-9} M for R6G) based on the CE mechanism where the rGO and the CT state formed at the interface of 1T- MoS_2 QDs and target molecules contribute to the SERS effect. Qiu et al.[155] prepared a heterosubstrate by decorating a wrinkled 2H-phase MoS_2 (W-MoS_2) platform with graphene microflowers (GMFs) exhibiting a LOD of 5×10^{-11} M for RhB. The authors suggested a combination of various factors behind the significant sensitivity, including (i) GMFs that served as molecular enrichers, (ii) enhanced interfacial interactions between the substrate and molecules, and (iii) S vacancies in W-MoS_2. Recently, mixed-dimensional (1D/2D) heterostructures (WO_{3-x}/WSe_2) were found to exhibit an attomolar level molecular sensitivity for methylene blue (MB). Lv et al. reported how an oxygen plasma treatment strategy can selectively convert the top WSe_2 layer to WO_{3-x} nanowires.[156] The ultrahigh performance stems from the efficient CT induced by the unique structures of 1D WO_{3-x} nanowires and the effective interlayer coupling of the heterostructures. In a study, a band structure-engineered $W_{18}O_{49}$/g-C_3N_4 heterostructure was found to exhibit notable enhancement as a CM-based SERS substrate. The heterojunction-induced efficient CT process, energy band matching resonance, and improved PICT efficiency via the oxygen vacancies in the $W_{18}O_{49}$ units accounted for the enhancement.[157] Recently, a report demonstrated a scheme for low-cost SERS sensing based on few-layered MoS_2−WS_2 nanocomposite structures. The formation of multiple inter- and intraflake heterojunctions introduces surface roughness to the substrate which yields a larger contact area between the substrate and the probe.[158] Higher adsorption of the analytes and an effective CT could be responsible for the enhancement. As mentioned in Section 3.3, the interlayer spacing of TMD can influence the SERS response of the materials. For graphene/MoS_2 vdW heterostructures, Chen et al. reported how the interlayer distances (<0.6 nm) impact the SERS response significantly.[159] A shorter interlayer distance exerts stronger vdW interactions that improve the dipole−dipole interaction and the CT and thereby yields a higher Raman enhancement.

3.5. MXenes as Candidates for SERS Substrates.

In the past decade, the family of 2D materials has further been enriched by the carbides, nitrides, or carbonitrides of transition metals known as MXenes.[160] The general formula of MXene is $M_{n+1}X_nT_x$, where the $n + 1$ layers of M cover n layers of X, forming $[MX]_nM$ arrangements. M, in the formula, stands for a transition metal or a combination of such, X is either C or N, T_x indicates the functional terminations on the outer transition metal layers (such as hydroxyl [OH], oxygen [O], fluorine [F], or other surface groups), and n ranges from 1 to 3. Since the first report on $Ti_3C_2T_x$ in 2011,[161] the MXene family has substantially increased and to date, dozens of MXenes have already been synthesized, and a potentially infinite number of compositions are possible. 2D MXenes exhibit several distinct features, for instance, metallic behavior, tunable electronic structure, biocompatibility, large surface area, rich surface chemistries, and SPRs in the visible or near-infrared range. The functionalized surfaces make MXenes hydrophilic and ready to bond to various species. Thus, they qualify for both EM and chemical enhancements in sensing applications and are now a fast-growing field in SERS. Generally, MXenes are produced by selectively etching the middle element (A) of the MAX phase structure, forming a multilayered structure of 2D MX with T_x; subsequently, the produced multilayer MXenes are separated into thin layers via intercalation-assisted liquid exfoliation by using sonication or by other methods.

3.5.1. MXenes Alone.

The most common MXene is titanium carbide, $Ti_3C_2T_x$.[162−166] $Ti_3C_2T_x$ exhibits a thickness-dependent SERS response and the enhancement depends on the adsorption and intercalation of dye molecules into the interlayer spacing.[165] Liu et al. developed a large-sized SERS-active substrate based on pristine monolayered $Ti_3C_2T_x$ nanosheets. Their large adsorption area added uniformity and stability to the substrate.[166] Among the various experimentally or theoretically possible MXenes, nitride-based MXenes are predicted to possess exceptional properties. Computational studies on nitride MXenes have shown a higher DOS at the Fermi level compared with those of carbides. However, the difficulty in the MAX ($M_{n+1}AN_n$) phase synthesis and also the poor stability issues of $M_{n+1}N_n$ layers in the employed etchant create complexity in nitride-based MXene synthesis. However, the selective etching of Al from the ternary layered Ti_2AlN (MAX) phase and intercalation by immersing the powder in a mixture of potassium fluoride and hydrochloric acid followed by sonication and centrifugation successfully synthesized few-layered Ti_2NT_x (M_2X-type) MXene. Soundiraraju and George found interesting SERS activity with the obtained nitride MXenes. An EF of 10^{12}

https://doi.org/10.1021/acsomega.4c06398
ACS Omega 2024, 9, 40242−40258

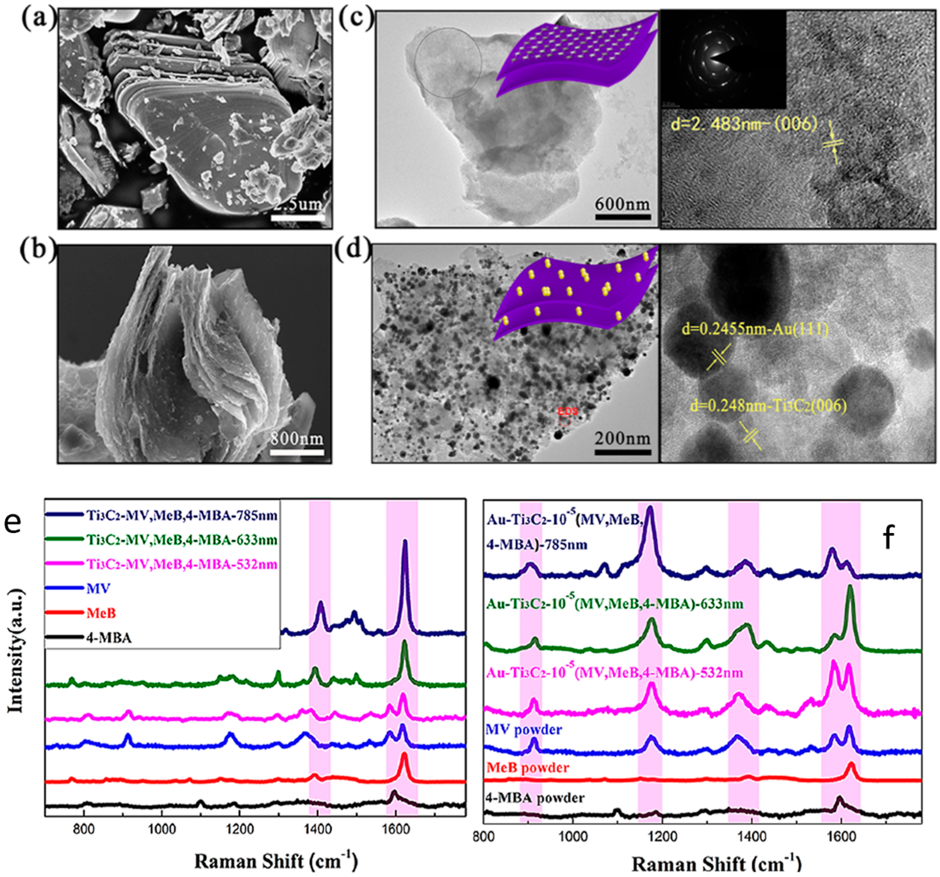

Figure 8. (a,b) SEM images of a Ti_3AlC_2 bulk structure (a) and Ti_3C_2 MXene (b). (c,d) TEM images, HRTEM images, and the corresponding SAED patterns (inset in the HRTEM images) of Ti_3C_2 MXene (c) and Au−Ti_3C_2 (d). (e,f) SERS spectra of 4-MBA, MeB, and MV powder; SERS spectra of the mixed solution with 10^{-5} M 4-MBA, MV, and MeB on Ti_3C_2 (e) and Au−Ti_3C_2 (f) substrates with different excitation lasers of 532, 633, and 785 nm. Reprinted with permission from ref 174. Copyright 2020 the author(s).

for R6G[167] indicates the potential of MXenes in replacing noble-metal-based SERS substrates. Bimetallic solid-solution MXene (TiVC) also showed ultrahigh sensitivity for R6G (EF of 10^{12} and femtomolar-level detection limit), dominated by the CM. The abundant DOS near the Fermi level of the TiVC and the strong interaction between the TiVC and analyte promoted the intermolecular CT resonance, resulting in significant enhancement.[168]

3.5.2. Metal−MXene Nanohybrids. A significant amount of research efforts have recently been exerted on MXene/metal nanostructures to combine the benefits of noble metal NPs and MXene.[169−172] Satheeshkumar et al. reported a one-step hybridization of silver, gold, and palladium NPs from solution onto exfoliated 2D Ti_3C_2 MXene nanosheets (Figure 7A) and demonstrated a higher sensitivity to MB dye for the hybrids compared to MB adsorbed on the MXene alone (Figure 7B).[169] Electrostatic self-assembly of a 2D electron gas (2DEG) titanium carbide ($Ti_3C_2T_x$) monolayer with Au NRs forms ($Ti_3C_2T_x$)/AuNRs hybrid platforms as positively charged AuNRs readily bound to the negatively charged $Ti_3C_2T_x$.[170] On adsorption of analytes on the MXene surface, the 2DEG provides an ideal channel for charge transport between $Ti_3C_2T_x$ and adsorbed analytes. PICT caused by $Ti_3C_2T_x$ structures and EM enhancement by AuNRs both add to the sensitive SERS activity. Yusoff et al. reported a superior enhancing ability of MXene/Ag nanostar composites compared to its components alone.[172] SERS substrates based on MXene can have diverse applications in food safety checking, biomedical sensing, etc.[63,173−175] For instance, Cui et al. designed a flexible SERS substrate for the detection of glucose levels in the tears of diabetic patients by growing Au NPs on the surface of $Ti_3C_2T_x$ nanosheets using a self-assembly technique. In another example, Chen et al. proposed MXene/AgNP films as nanocarriers for SERS-traceable drug delivery.[176] $Ti_3C_2T_x$ and AuNP assemblies displayed their potential for detecting trace contaminants (AFB1) in agricultural products.[175] Ti_3C_2 and Au−Ti_3C_2 substrates have been reported to exhibit selectivity on different probe molecules at different excitation wavelengths, which can facilitate the detection of target probe molecules in complex solution environments (see Figure 8).[174] Yoo et al.[177] reported the activity of MXene-blanketed Au NP assembly as a SERS platform. The MXene layer enables an efficient CT effect, while wrinkled surface structures generated from the blanketing of the MXene layer over the Au NP assembly facilitate an increase in the EM effect by guiding the analyte to be captured near the hotspot between Au NPs. Recently, a study reported the activity of $Ti_3C_2T_x$ MXene@GO/Au nanoclusters as a SERS substrate.[178]

As compared to regular $Ti_3C_2T_x$, reduced $Ti_3C_2T_x$ MXene (r-$Ti_3C_2T_x$) has shown an order of magnitude higher SERS EF (see Figure 9). A larger number of surface-Ti atoms exposed due to the loss of F terminations allow a larger population of dye molecules to interact with r-$Ti_3C_2T_x$. The increased electronic DOS at the Fermi level facilitates the CT interaction between the r-$Ti_3C_2T_x$ MXene surface and probe molecules and contributes to the improved SERS activity as well.[179]

https://doi.org/10.1021/acsomega.4c06398
ACS Omega 2024, 9, 40242−40258

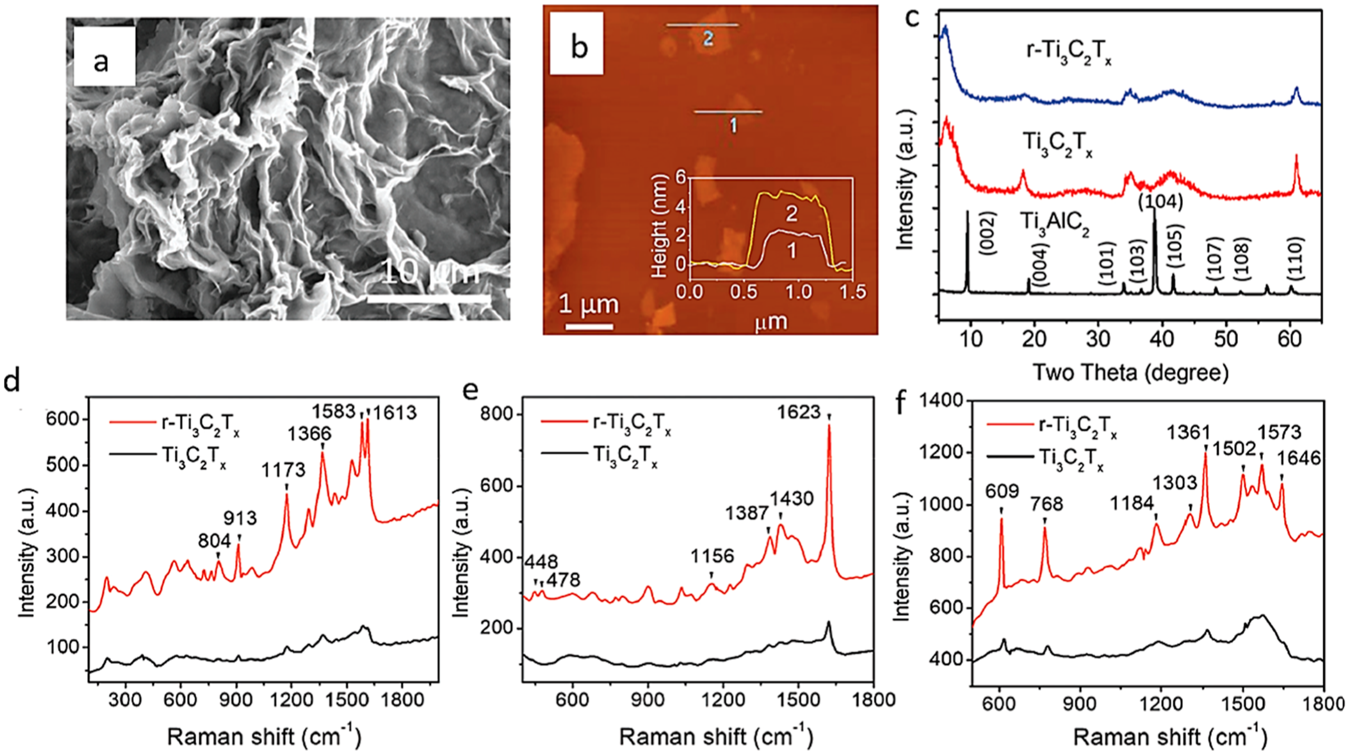

Figure 9. (a) SEM micrographs of the r-$Ti_3C_2T_x$ powder. (b) Tapping mode AFM image of $Ti_3C_2T_x$ nanosheets on SiO_2/Si. (c) XRD patterns of the Ti_3AlC_2 MAX phase (black), $Ti_3C_2T_x$ (red), and r-Ti3C2Tx (blue). SERS spectra of the probe molecules: (d) crystal violet at 2×10^{-6} M, (e) MB at 1×10^{-6} M, and (f) rhodamine 6G (R6G) at 1×10^{-7} M, respectively, collected on $Ti_3C_2T_x/SiO_2$/Si (black) and r-$Ti_3C_2T_x/SiO_2$/Si (red) substrates. Used with permission of The Royal Society of Chemistry, from ref 179; permission conveyed through Copyright Clearance Center, Inc.

MXenes and their hybrid compounds are still in their early stages. Although the number of methods used to synthesize MXenes has expanded, most are heavily reliant on the selective etching of the middle element (A) of the MAX-phase precursors using hazardous solutions, including hydrofluoric acid. Further investigations toward the efficient synthesis of other MXene types can yield more possibilities for 2D MXene-based excellent SERS substrates, either alone or in nanocomposite form.

4. MECHANISMS BEHIND CES

The significance of the CT mechanism in the 2D material-based substrates has nicely been verified by introducing an insulating (thin Al_2O_3) layer between a 2D layered substrate (1L-$PdSe_2$) and an analyte (R6G molecules), as such an arrangement (i.e., R6G on Al_2O_3/1L-$PdSe_2$) did not result in any detectable R6G peaks, whereas R6G molecules on monolayer $PdSe_2$ achieved a detection limit of 10^{-9} M with an EF of 10^5.[180] The degree of CE would depend on the adsorption of the target molecules on the substrate. Physisorption occurs when molecules attach to the surface of the adsorbent by relatively weak forces, such as vdW forces or dipole-driven interactions, and typically does not result in a chemical reaction, while chemisorption refers to a stronger adsorbate−adsorbent interaction process that leads to the formation of chemical bonds and changes in the electronic structure of bonding atoms or molecules and influences the enhancement at a different level. The possible situations in the CT mechanism are summarized here: (1) a resonance effect where the incident beam matches with the molecular excitation; (2) a CT effect when the incident light is in resonance with a metal−molecule or molecule−metal transition;[181,182] and (3) ground state interactions between the substrate and the analyte, i.e., where the process does not depend on the excitation laser wavelength. Thus, the electronic structure of the analyte becomes crucial to a CM-induced SERS effect, while it is less significant to the EM mechanism. In the case of a molecule−metal system, the CT between the HOMO level of analyte molecules and the Fermi level of metal could play a decisive role. However, for semiconducting materials, the CT scheme involves the VB and CB edges. Also, studies indicated an asymmetric nature of the CM effect. Kim et al. suggested a preferential route to attain a large CM EF. The calculated EF for a transition associated with semiconductor substrates to a molecular LUMO was found to be at least 100 times larger than that for a transition from the HOMO to CB.[182] The phase state (2H or 1T) of the TMD also plays a dominant role in the CT mechanism. Compared to the 2H phase, 1T-MoS_2 has higher-lying Fermi electrons that could migrate into the HOMO level without extra energy, leading to a higher SERS response. Moreover, the engineered/modified energy levels of semiconductor substrates can influence the PICT process. For instance, partially oxidized MoS_2 (band gap 0.56 eV) provided substantial advantages over pristine MoS_2 (band gap 1.29 eV) and fully oxidized MoO_3 (band gap 3.1 eV) samples (see Figure 6B).[138] For both pristine MoS_2 and partially oxidized MoS_2 materials, CT transitions from the VB to LUMO are possible, while the downshifted VB position after oxygen incorporation in partially oxidized MoS_2 makes CT transition energy (2.26 eV) much closer to the excitation laser energy (2.33 eV) which improves the CT efficiency and promotes its contribution to SERS enhancement.

Though the CT mechanism (as discussed in the above sections) is involved in most substrates, it fails to explain all CE effects in 2D materials, such as the enhancement effect of h-BN where a large band gap of more than 5.9 eV leads toward insignificant CT capacity. However, highly polar B−N bonds induce symmetry perturbation in the probe (CuPc) molecules by interface dipole interaction which mainly drives the enhancement.[33] This mechanism has been further recognized by several subsequent studies. The direction of substrate dipoles impacts dipole−dipole interactions significantly. Substrates with effective out-of-plane dipoles have the highest chance of being SERS-active. Due to their highly symmetric structures, common 2D materials do not typically carry atomic-scale dipoles in the out-of-plane direction. Recently, asymmetrical Janus TMDs with dissimilar chalcogen atoms on each side earned considerable research attention. Synthesis is based on the atomic substitution of TMD's surface atoms. Half of the chalcogen atoms (either the top or bottom side) are substituted by different types of chalcogen atoms, thus, breaking the out-of-plan symmetry. For example, the Janus structure of MoSSe with Mo in the middle and a layer of S on one side and Se on the other creates an intrinsic dipole that exists along the vertical direction of the structure. The generated electric field interacts with adsorbed molecules and that qualifies for strong dipole interactions between the substrate and molecules. A recent study by Lou et al. demonstrated the detection of biomolecules (glucose) via dipole-interaction-driven SERS phenomena. Glucose has different vibrational modes with different orientations and interacts differently with the dipoles associated with the substrate (monolayer Janus MoSSe) and yields a variation in enhancements.[183] Therefore, for a given CE system, many factors can come into play, including DOS, orientation of molecules on the substrate surface, presence of excitonic levels, etc. which are not always easy to single out or separate and make the chemical effect relatively complex.

5. CONCLUSIONS

SERS has witnessed a long way—evolving from crude roughened metal electrodes to low-dimensional systems (regular metallic or nonmetallic structures) with tailored physical and/or chemical properties. In earlier studies, attention was largely concentrated on the improvement of EFs. The distribution of molecules in the vicinity of the EM hotspots is quite complicated, and the number of molecules near the hotspots can fluctuate. Thus, substrate synthesis with optimized EFs is not the only challenge, but reproducing the amplified signal of the investigated sample with uniformity is another important criterion. Hence, researchers gradually shifted their attention to resolving such issues. A rich variety of substrate preparation techniques was exemplified by several reports. However, on the way toward commercialization or for routine practice in research laboratories, SERS demands more attention toward other factors as well, including a low manufacturing cost, ease of mass production, sustainability, stability, etc. where 2D materials with distinct characteristics can show their strength. Nevertheless, high sensitivity is a key factor in the SERS performance. Signal enhancements from 2D materials are generally not as high as those obtained with silver or gold substrates and, thus, are insufficient to meet the requirements for detection applications beyond certain limits. Composites of 2D materials with traditional metallic nanostructures are sometimes much more attractive choices than their counterparts alone. Metal/TMD hybrid substrates could exploit better uniformity, good adsorption ability, and fluorescence quenching efficiency from the 2D materials, while metallic nanostructures add high detection sensitivity to the substrate. Developing more sophisticated hybrid substrate designs could drive the SERS sensing operation up a level in real situations. The SERS performance of a substrate is usually evaluated using MB, CV, R6G, etc. dyes. Going beyond such common probes and testing the performance in complex mixtures and more reactive environments become vital from a practical implementation aspect.

Positioning the energy levels of 2D materials suitably with the probe molecules via defect introduction and engineering could lead to a notable SERS effect. Such an adjustment of the energy levels and band structures is challenging. Moreover, the thickness- and morphology-dependent enhancement mechanism of 2D materials is yet unclear, which motivates further investigation. The diverse range of TMDs provides considerable flexibility; however, special treatments or notable research strategies have largely been limited to prototype material, MoS_2. Expanding the range of SERS materials, such as MXenes, could also provide much room for further SERS studies. The scope for modification of surface terminations makes MXenes especially appealing. Exploring MXenes beyond Ti_3C2T_x, identifying new precursors (beyond MAX phases), and the realization of an interflake charge-transport mechanism may widen the promises of the SERS technique. Moreover, as the probability of electron transition is linearly correlated with the DOS around the Fermi level, layered semimetallic TMDs (with abundant DOS near the Fermi level) have recently been explored as noble-metal-comparable substrates. A controllable synthesis of such substrates could stimulate their use as ideal plasmon-free SERS platforms.

■ AUTHOR INFORMATION

Corresponding Author

Dipanwita Majumdar − *Satyendra Nath Bose National Centre for Basic Sciences, Kolkata 700106, India;* orcid.org/0000-0002-1519-0762; Email: dipanwitamajumdar27@gmail.com

Complete contact information is available at:
https://pubs.acs.org/10.1021/acsomega.4c06398

Notes

The author declares no competing financial interest.

■ ACKNOWLEDGMENTS

This work was supported by the Department of Science and Technology, Govt. of India (DST/INSPIRE/04/2016/002377).

■ REFERENCES

(1) Fleischmann, M.; Hendra, P. J.; McQuillan, A. J. Raman Spectra of Pyridine Adsorbed at a Silver Electrode. *Chem. Phys. Lett.* **1974**, *26*, 163−166.

(2) Jeanmaire, D. L.; Van Duyne, R. P. Surface raman spectroelectrochemistry: Part I. Heterocyclic, aromatic, and aliphatic amines adsorbed on the anodized silver electrode. *J. Electroanal. Chem. Interfacial Electrochem.* **1977**, *84*, 1−20.

(3) Albrecht, M. G.; Creighton, J. A. Anomalously Intense Raman Spectra of Pyridine at a Silver Electrode. *J. Am. Chem. Soc.* **1977**, *99*, 5215−5217.

(4) Moskovits, M. Surface Roughness and the Enhanced Intensity of Raman Scattering by Molecules Adsorbed on Metals. *J. Chem. Phys.* **1978**, *69*, 4159−4161.

(5) Stiles, P. L.; Dieringer, J. A.; Shah, N. C.; Van Duyne, R. P. Surface-enhanced Raman spectroscopy. *Annu. Rev. Anal. Chem.* **2008**, *1*, 601−626.

(6) Baik, S. Y.; Cho, Y. J.; Lim, Y. R.; Im, H. S.; Jang, D. M.; Myung, Y.; Park, J.; Kang, H. S. Charge-Selective Surface-Enhanced Raman

Scattering Using Silver and Gold Nanoparticles Deposited on Silicon-Carbon Core-Shell Nanowires. *ACS Nano* **2012**, *6*, 2459−2470.

(7) Liu, D.; Zhou, F.; Li, C.; Zhang, T.; Zhang, H.; Cai, W.; Li, Y. Black Gold: Plasmonic colloidosomes with broadband absorption self-assembled from monodispersed gold nanospheres by using a reverse emulsion system. *Angew. Chem., Int. Ed.* **2015**, *54*, 9596−9600.

(8) Otto, A. The 'chemical' (electronic) contribution to surface-enhanced Raman scattering. *J. Raman Spectrosc.* **2005**, *36*, 497−509.

(9) Persson, B. N. J.; Zhao, K.; Zhang, Z. Y. Chemical contribution to surface-enhanced Raman scattering. *Phys. Rev. Lett.* **2006**, *96*, 207401.

(10) Morton, S. M.; Jensen, L. Understanding the Molecule−Surface Chemical Coupling in SERS. *J. Am. Chem. Soc.* **2009**, *131* (11), 4090−4098.

(11) Creighton, J. A.; Blatchford, C. G.; Albrecht, M. G. Plasma resonance enhancement of Raman scattering by pyridine adsorbed on silver or gold sol particles of size comparable to the excitation wavelength. *J. Chem. Soc., Faraday Trans. 2* **1979**, *75*, 790−798.

(12) Hildebrandt, P.; Stockburger, M. Surface-Enhanced Resonance Raman Spectroscopy of Rhodamine 6G Adsorbed on Colloidal Silver. *J. Phys. Chem.* **1984**, *88*, 5935−5944.

(13) Michaels, A. M.; Nirmal, M.; Brus, L. Surface enhanced Raman spectroscopy of individual Rhodamine 6G molecules on large Ag nanocrystals. *J. Am. Chem. Soc.* **1999**, *121* (43), 9932−9939.

(14) Yang, Y.; Li, Z. Y.; Yamaguchi, K.; Tanemura, M.; Huang, Z. R.; Jiang, D.; Chen, Y.; Zhou, F.; Nogami, M. Controlled fabrication of silver nanoneedles array for SERS and their application in rapid detection of narcotics. *Nanoscale* **2012**, *4* (8), 2663−2669.

(15) Guselnikova, O.; Nugraha, A. S.; Na, J.; Postnikov, P.; Kim, H.-J.; Plotnikov, E.; Yamauchi, Y. Surface Filtration in Mesoporous Au Films Decorated by Ag Nanoparticles for Solving SERS Sensing Small Molecules in Living Cells. *ACS Appl. Mater. Interfaces* **2022**, *14* (36), 41629−41639.

(16) Yao, X.; Jiang, S.; Luo, S.; Liu, B. W.; Huang, T. X.; Hu, S.; Zhu, J.; Wang, X.; Ren, B. Uniform Periodic Bowtie SERS Substrate with Narrow Nanogaps Obtained by Monitored Pulsed Electrodeposition. *ACS Appl. Mater. Interfaces* **2020**, *12* (32), 36505−36512.

(17) Nie, S.; Emory, S. R. Probing single molecules and single nanoparticles by surface-enhanced Raman scattering. *Science* **1997**, *275* (5303), 1102−1106.

(18) Kneipp, K.; Wang, Y.; Kneipp, H.; Perelman, L. T.; Itzkan, I.; Dasari, R. R.; Feld, M. S. Single Molecule Detection Using Surface-Enhanced Raman Scattering (SERS). *Phys. Rev. Lett.* **1997**, *78*, 1667−1670.

(19) Petryayeva, E.; Krull, U. J. Localized surface plasmon resonance: nanostructures, bioassays and biosensing-a review. *Anal. Chim. Acta* **2011**, *706*, 8−24.

(20) Kelly, K. L.; Coronado, E.; Zhao, L. L.; Schatz, G. C. The optical properties of metal nanoparticles: the influence of size, shape, and dielectric environment. *J. Phys. Chem. B* **2003**, *107*, 668−677.

(21) Suzuki, M.; Niidome, Y.; Kuwahara, Y.; Terasaki, N.; Inoue, K.; Yamada, S. Surface-enhanced nonresonance Raman scattering from size-and morphology-controlled gold nanoparticle films. *J. Phys. Chem. B* **2004**, *108*, 11660−11665.

(22) Bell, S. E. J.; McCourt, M. R. SERS enhancement by aggregated Au colloids: effect of particle size. *Phys. Chem. Chem. Phys.* **2009**, *11*, 7455−7462.

(23) Yang, Y.; Zhang, Q.; Fu, Z.; Qin, D. Transformation of Ag Nanocubes into Ag-Au Hollow Nanostructures with Enriched Ag Contents to Improve SERS Activity and Chemical Stability. *ACS Appl. Mater. Interfaces* **2014**, *6*, 3750−3757.

(24) Yang, Y.; Liu, J.; Fu, Z.; Qin, D. Galvanic Replacement-Free Deposition of Au on Ag for Core-Shell Nanocubes with Enhanced Chemical Stability and SERS Activity. *J. Am. Chem. Soc.* **2014**, *136*, 8153−8156.

(25) Mai, F.-D.; Yang, K.-H.; Liu, Y.-C.; Hsu, T.-C. Improved Stabilities on Surface-Enhanced Raman Scattering-Active Ag/Al_2O_3 Films on Substrates. *Analyst* **2012**, *137*, 5906−5912.

(26) Yang, K.-H.; Liu, Y.-C.; Hsu, T.-C.; Juang, M.-Y. Strategy to Improve Stability of Surface-Enhanced Raman Scattering-Active Ag Substrates. *J. Mater. Chem.* **2010**, *20*, 7530−7535.

(27) Ling, X.; Xie, L.; Fang, Y.; Xu, H.; Zhang, H.; Kong, J.; Dresselhaus, M. S.; Zhang, J.; Liu, Z. Can graphene be used as a substrate for Raman enhancement? *Nano Lett.* **2010**, *10*, 553−561.

(28) Ling, X.; Zhang, J. First-layer effect in graphene-enhanced Raman scattering. *Small* **2010**, *6* (18), 2020−2025.

(29) Xu, W.; Mao, N.; Zhang, J. Graphene: A Platform for Surface-Enhanced Raman Spectroscopy. *Small* **2013**, *9* (8), 1206−1224.

(30) Huh, S.; Park, J.; Kim, Y. S.; Kim, K. S.; Hong, B. H.; Nam, J.-M. UV/Ozone-Oxidized Large-Scale Graphene Platform with Large Chemical Enhancement in Surface-Enhanced Raman Scattering. *ACS Nano* **2011**, *5* (12), 9799−9806.

(31) Chugh, D.; Jagadish, C.; Tan, H. Large-area hexagonal boron nitride for surface enhanced Raman spectroscopy. *Adv. Mater. Technol.* **2019**, *4*, 1900220.

(32) Kundu, A.; Rani, R.; Hazra, K. S. Controlled nanofabrication of metal-free SERS substrate on few layered black phosphorus by low power focused laser irradiation. *Nanoscale* **2019**, *11* (35), 16245−16252.

(33) Ling, X.; Fang, W.; Lee, Y. H.; Araujo, P. T.; Zhang, X.; Rodriguez-Nieva, J. F.; Lin, Y.; Zhang, J.; Kong, J.; Dresselhaus, M. S. Raman enhancement effect on two-dimensional layered materials: graphene, h-BN and MoS_2. *Nano Lett.* **2014**, *14*, 3033−3040.

(34) Xu, Y. Y.; Yang, C.; Jiang, S. Z.; Man, B. Y.; Liu, M.; Chen, C. S.; Zhang, C.; Sun, Z. C.; Qiu, H. W.; Li, H. S.; Feng, D. J.; Zhang, J. X. Layer-controlled large area MoS_2 layers grown on mica substrate for surface-enhanced Raman scattering. *Appl. Surf. Sci.* **2015**, *357*, 1708−1713.

(35) Lv, Q.; Tan, J.; Wang, Z.; Yu, L.; Liu, B.; Lin, J.; Li, J.; Huang, Z.-H.; Kang, F.; Lv, R. Femtomolar-Level Molecular Sensing of Monolayer Tungsten Diselenide Induced by Heteroatom Doping with Long-Term Stability. *Adv. Funct. Mater.* **2022**, *32* (34), 2200273.

(36) Yin, Y.; Miao, P.; Zhang, Y.; Han, J.; Zhang, X.; Gong, Y.; Gu, L.; Xu, C.; Yao, T.; Xu, P.; et al. Significantly increased Raman enhancement on MoX_2 (X = S, Se) monolayers upon phase transition. *Adv. Funct. Mater.* **2017**, *27*, 1606694.

(37) Yan, D.; Qiu, W.; Chen, X.; Liu, L.; Lai, Y.; Meng, Z.; Song, J.; Liu, Y.; Liu, X.-Y.; Zhan, D. Achieving High-Performance Surface-Enhanced Raman Scattering through One-Step Thermal Treatment of Bulk MoS_2. *J. Phys. Chem. C* **2018**, *122*, 14467−14473.

(38) Wang, Y.; Ni, Z.; Hu, H.; Hao, Y.; Wong, C. P.; Yu, T.; Thong, J. T.; Shen, Z. X. Gold on Graphene as a Substrate for Surface Enhanced Raman Scattering Study. *Appl. Phys. Lett.* **2010**, *97*, 163111.

(39) Zhou, H.; Qiu, C.; Yu, F.; Yang, H.; Chen, M.; Hu, L.; Sun, L. Thickness-Dependent Morphologies and Surface-Enhanced Raman Scattering of Ag Deposited on n-Layer Graphenes. *J. Phys. Chem. C* **2011**, *115*, 11348−11354.

(40) Sidorov, A. N.; Sławiński, G. W.; Jayatissa, A. H.; Zamborini, F. P.; Sumanasekera, G. U. A surface-enhanced Raman spectroscopy study of thin graphene sheets functionalized with gold and silver nanostructures by seed-mediated growth. *Carbon* **2012**, *50* (2), 699−705.

(41) Wang, X.; Wang, N.; Gong, T.; Zhu, Y.; Zhang, J. Preparation of Graphene-Ag Nanoparticles Hybrids and Their SERS Activities. *Appl. Surf. Sci.* **2016**, *387*, 707−719.

(42) Xu, S.; Jiang, S.; Wang, J.; Wei, J.; Yue, W.; Ma, Y. Graphene Isolated Au Nanoparticle Arrays with High Reproducibility for High-Performance Surface-Enhanced Raman Scattering. *Sens. Actuators, B* **2016**, *222*, 1175−1183.

(43) Jiang, J.; Zou, J.; Wee, A. T. S.; Zhang, W. Use of Single-Layer g-C_3N_4/Ag Hybrids for Surface-Enhanced Raman Scattering (SERS). *Sci. Rep.* **2016**, *6*, 34599.

(44) Wang, J.; Liu, R.; Zhang, C.; Han, G.; Zhao, J.; Liu, B.; Jiang, C.; Zhang, Z. Synthesis of g-C_3N_4 nanosheet/Au@Ag nanoparticle hybrids as SERS probes for cancer cell diagnostics. *RSC Adv.* **2015**, *5*, 86803−86810.

(45) Zhang, H.; Li, G.; Li, S.; Xu, L.; Tian, Y.; Jiao, A.; Liu, X.; Chen, F.; Chen, M. Boron nitride/gold nanocomposites for crystal violet and creatinine detection by surface-enhanced Raman spectroscopy. *Appl. Surf. Sci.* **2018**, *457*, 684−694.
(46) Lin, Y.; Bunker, C. E.; Fernando, K. A. S.; Connell, J. W. Aqueously Dispersed Silver Nanoparticle-Decorated Boron Nitride Nanosheets for Reusable, Thermal Oxidation-Resistant Surface Enhanced Raman Spectroscopy (SERS) Devices. *ACS Appl. Mater. Interfaces* **2012**, *4* (2), 1110−1117.
(47) Yang, S.; Zhang, Z.; Zhao, J.; Zheng, H. High surface enhanced Raman scattering activity of BN nanosheets−Ag nanoparticles hybrids. *J. Alloys Compd.* **2014**, *583*, 231−236.
(48) Yang, G.; Liu, Z.; Li, Y.; Hou, Y.; Fei, X.; Su, C.; Wang, S.; Zhuang, Z.; Guo, Z. Facile synthesis of black phosphorus−Au nanocomposites for enhanced photothermal cancer therapy and surface-enhanced Raman scattering analysis. *Biomater. Sci.* **2017**, *5*, 2048−2055.
(49) Lin, C.; Liang, S.; Peng, Y.; Long, L.; Li, Y.; Huang, Z.; Long, N. V.; Luo, X.; Liu, J.; Li, Z.; Yang, Y. Visualized SERS Imaging of Single Molecule by Ag/Black Phosphorus Nanosheets. *Nano-Micro Lett.* **2022**, *14*, 75.
(50) Kim, J.; Byun, S.; Smith, A. J.; Yu, J.; Huang, J. Enhanced Electrocatalytic Properties of Transition-Metal Dichalcogenides Sheets by Spontaneous Gold Nanoparticle Decoration. *J. Phys. Chem. Lett.* **2013**, *4* (8), 1227−1232.
(51) Li, J.; Zhang, W.; Lei, H.; Li, B. Ag nanowire/nanoparticle-decorated MoS_2 monolayers for surface-enhanced Raman scattering applications. *Nano Res.* **2018**, *11* (4), 2181−2189.
(52) Pramanik, A.; Davis, D.; Patibandla, S.; Begum, S.; Ray, P.; Gates, K.; Gao, Y.; Chandra Ray, P. A WS_2-gold nanoparticle heterostructure-based novel SERS platform for the rapid identification of antibiotic-resistant pathogens. *Nanoscale Adv.* **2020**, *2*, 2025−2033.
(53) Majumdar, D.; Jana, S.; Ray, S. K. Gold nanoparticles decorated 2D-WSe_2 as a SERS substrate. *Spectrochim. Acta, Part A* **2022**, *278*, 121349.
(54) Pyrak, E.; Krajczewski, J.; Kowalik, A.; Kudelski, A.; Jaworska, A. Surface enhanced Raman spectroscopy for DNA biosensors—how far are we? *Molecules* **2019**, *24* (24), 4423.
(55) Liu, T.; Tsai, K. T.; Wang, H. H.; Chen, Y.; Chen, Y. H.; Chao, Y. C.; Chang, H. H.; Lin, C. H.; Wang, J. K.; Wang, Y. L. Functionalized Arrays of Raman-Enhancing Nanoparticles for Capture and Culture-Free Analysis of Bacteria in Human Blood. *Nat. Commun.* **2011**, *2*, 538.
(56) Cao, Y. C.; Jin, R. C.; Mirkin, C. A. Nanoparticles with Raman spectroscopic fingerprints for DNA and RNA detection. *Science* **2002**, *297*, 1536−1540.
(57) Wang, H.-H.; Cheng, T. Y.; Sharma, P.; Chiang, F. Y.; Chiu, S. W. Y.; Wang, J. K.; Wang, Y. L. Transparent Raman-enhancing substrates for microbiological monitoring and *in situ* pollutant detection. *Nanotechnology* **2011**, *22*, 385702.
(58) Peksa, V.; Jahn, M.; Štolcová, L.; Schulz, V.; Proška, J.; Procházka, M.; Weber, K.; Cialla-May, D.; Popp, J. Quantitative SERS Analysis of Azorubine (E 122) in Sweet Drinks. *Anal. Chem.* **2015**, *87*, 2840−2844.
(59) Nilghaz, A.; Mahdi Mousavi, S.; Amiri, A.; Tian, J.; Cao, R.; Wang, X. Surface-Enhanced Raman Spectroscopy Substrates for Food Safety and Quality Analysis. *J. Agric. Food Chem.* **2022**, *70* (18), 5463−5476.
(60) Fisher, K. M.; McLeish, J. A.; Jamieson, L. E.; Jiang, J.; Hopgood, J. R.; McLaughlin, S.; Donaldson, K.; Campbell, C. J. SERS as a tool for *in vitro* toxicology. *Faraday Discuss.* **2016**, *187*, 501−520.
(61) Yang, Y.; Li, Z. Y.; Yamaguchi, K.; Tanemura, M.; Huang, Z. R.; Jiang, D.; Chen, Y.; Zhou, F.; Nogami, M. Controlled fabrication of silver nanoneedles array for SERS and their application in rapid detection of narcotics. *Nanoscale* **2012**, *4* (8), 2663−2669.
(62) Muehlethaler, C.; Leona, M.; Lombardi, J. R. Review of Surface Enhanced Raman Scattering Applications in Forensic Science. *Anal. Chem.* **2016**, *88* (1), 152−169.
(63) Cui, X.; Li, J.; Li, Y.; Liu, M.; Qiao, J.; Wang, D.; Cao, H.; He, W.; Feng, Y.; Yang, Z. Detection of glucose in diabetic tears by using gold nanoparticles and MXene composite surface-enhanced Raman scattering substrates. *Spectrochim. Acta, Part A* **2022**, *266*, 120432.
(64) Wang, Y.; Zhao, P.; Mao, L.; Hou, Y.; Li, D. Determination of brain injury biomarkers by surface-enhanced Raman scattering using hollow gold nanospheres. *RSC Adv.* **2018**, *8*, 3143−3150.
(65) Zhou, W.; Gao, X.; Liu, D.; Chen, X. Gold Nanoparticles for *In Vitro* Diagnostics. *Chem. Rev.* **2015**, *115*, 10575−10636.
(66) Hidi, I. J.; Jahn, M.; Pletz, M. W.; Weber, K.; Cialla-May, D.; Popp, J. Toward Levofloxacin Monitoring in Human Urine Samples by Employing the LoC-SERS Technique. *J. Phys. Chem. C* **2016**, *120*, 20613−20623.
(67) Chon, H.; Lee, S.; Yoon, S. Y.; Lee, E. K.; Chang, S. I.; Choo, J. SERS-based competitive immunoassay of troponin I and CK-MB markers for early diagnosis of acute myocardial infarction. *Chem. Commun.* **2014**, *50*, 1058−1060.
(68) Xu, H.; Aizpurua, J.; Kall, M.; Apell, P. Electromagnetic contributions to single-molecule sensitivity in surface-enhanced Raman scattering. *Phys. Rev. E* **2000**, *62*, 4318−4324.
(69) Stockman, M. I. Electromagnetic Theory of SERS. In *Surface-Enhanced Raman Scattering*; Kneipp, K.; Moskovits, M.; Kneipp, H., Eds.; *Topics in Applied Physics*; Springer: Berlin, Heidelberg, 2006; Vol. *103*.
(70) Wustholz, K. L.; Brosseau, C. L.; Casadio, F.; Van Duyne, R. P. Surface-enhanced Raman spectroscopy of dyes: from single molecules to the artists' canvas. *Phys. Chem. Chem. Phys.* **2009**, *11*, 7350−7359.
(71) Ding, S.-Y.; You, E.-M.; Tian, Z.-Q.; Moskovits, M. Electromagnetic theories of surface-enhanced Raman spectroscopy. *Chem. Soc. Rev.* **2017**, *46*, 4042−4076.
(72) Schlücker, S. Surface-Enhanced Raman Spectroscopy: Concepts and Chemical Applications. *Angew. Chem., Int. Ed.* **2014**, *53* (19), 4756−4795.
(73) Camden, J. P.; Dieringer, J. A.; Wang, Y.; Masiello, D. J.; Marks, L. D.; Schatz, G. C.; Van Duyne, R. P. Probing the structure of single-molecule surface-enhanced Raman scattering hot spots. *J. Am. Chem. Soc.* **2008**, *130*, 12616−12617.
(74) Rycenga, M.; Camargo, P. H. C.; Li, W.; Moran, C. H.; Xia, Y. Understanding the SERS Effects of Single Silver Nanoparticles and Their Dimers, One at a Time. *J. Phys. Chem. Lett.* **2010**, *1* (4), 696−703.
(75) Diebold, E. D.; Peng, P.; Mazur, E. Isolating surface-enhanced Raman scattering hot spots using multiphoton lithography. *J. Am. Chem. Soc.* **2009**, *131*, 16356−16357.
(76) Petti, L.; Capasso, R.; Rippa, M.; Pannico, M.; La Manna, P.; Peluso, G.; Calarco, A.; Bobeico, E.; Musto, P. A plasmonic nanostructure fabricated by electron beam lithography as a sensitive and highly homogeneous SERS substrate for bio-sensing applications. *Vib. Spectrosc.* **2016**, *82*, 22−30.
(77) Yue, W.; Wang, Z.; Yang, Y.; Chen, L.; Syed, A.; Wong, K.; Wang, X. Electron-beam lithography of gold nanostructures for surface-enhanced Raman scattering. *J. Manuf. Syst.* **2012**, *22* (12), 125007.
(78) Mikac, L.; Ivanda, M.; Gotić, M.; Mihelj, T.; Horvat, L. Synthesis and characterization of silver colloidal nanoparticles with different coatings for SERS application. *J. Nanopart. Res.* **2014**, *16*, 2748.
(79) Munro, C. H.; Smith, W. E.; Garner, M.; Clarkson, J.; White, P. C. Characterization of the Surface of a Citrate-Reduced Colloid Optimized for Use as a Substrate for Surface-Enhanced Resonance Raman Scattering. *Langmuir* **1995**, *11* (10), 3712−3720.
(80) Athira, K.; Ranjana, M.; Bharathi, M. S. S.; Narasimha Reddy, B.; Satheesh Babu, T.; Venugopal Rao, S.; Ravi Kumar, D. V. Aggregation induced, formaldehyde tailored nanowire like networks of Cu and their SERS activity. *Chem. Phys. Lett.* **2020**, *748*, 137390.
(81) Chang, Y.-L.; Su, C.-J.; Lu, L.-C.; Wan, D. Aluminum Plasmonic Nanoclusters for Paper-Based Surface-Enhanced Raman Spectroscopy. *Anal. Chem.* **2022**, *94* (47), 16319−16327.
(82) Cai, W.; Ren, B.; Li, X.; She, C.; Liu, F.; Cai, X.; Tian, Z. Investigation of surface-enhanced Raman scattering from platinum electrodes using a confocal Raman microscope: Dependence of surface roughening pretreatment. *Surf. Sci.* **1998**, *406*, 9−22.
(83) Liu, Z.; Yang, Z.; Cui, L.; Ren, B.; Tian, Z. Electrochemically roughened palladium electrodes for surface-enhanced Raman spec-

troscopy: Methodology, mechanism, and application. *J. Phys. Chem. C* **2007**, *111*, 1770−1775.

(84) Guo, L.; Huang, Q.; Li, X.-Y.; Yang, S. Iron nanoparticles: Synthesis and applications in surface enhanced Raman scattering and electrocatalysis. *Phys. Chem. Chem. Phys.* **2001**, *3*, 1661−1665.

(85) Zhang, C.; Jiang, S. Z.; Yang, C.; Li, C. H.; Huo, Y. Y.; Liu, X. Y.; Liu, A. H.; Wei, Q.; Gao, S. S.; Gao, X. G.; Man, B. Y. Gold@silver bimetal nanoparticles/pyramidal silicon 3D substrate with high reproducibility for high-performance SERS. *Sci. Rep.* **2016**, *6*, 25243.

(86) Zhang, T.; Sun, Y.; Hang, L.; Li, H.; Liu, G.; Zhang, X.; Lyu, X.; Cai, W.; Li, Y. Periodic Porous Alloyed Au−Ag Nanosphere Arrays and Their Highly Sensitive SERS Performance with Good Reproducibility and High Density of Hotspots. *ACS Appl. Mater. Interfaces* **2018**, *10* (11), 9792−9801.

(87) Capaccio, A.; Sasso, A.; Rusciano, G. A simple and reliable approach for the fabrication of nanoporous silver patterns for surface-enhanced Raman spectroscopy applications. *Sci. Rep.* **2021**, *11*, 22295.

(88) Wang, B.; Zhang, L.; Zhou, X. Synthesis of silver nanocubes as a SERS substrate for the determination of pesticide paraoxon and thiram. *Spectrochim. Acta, Part A* **2014**, *121*, 63−69.

(89) Saute, B.; Premasiri, R.; Ziegler, L.; Narayanan, R. Gold nanorods as surface enhanced Raman spectroscopy substrates for sensitive and selective detection of ultra-low levels of dithiocarbamate pesticides. *Analyst* **2012**, *137*, 5082−5087.

(90) Khoury, C. G.; Vo-Dinh, T. Gold Nanostars For Surface-Enhanced Raman Scattering: Synthesis, Characterization and Optimization. *J. Phys. Chem. C* **2008**, *112* (48), 18849−18859.

(91) Tao, Q.; Li, S.; Ma, C.; Liu, K.; Zhang, Q.-Y. A highly sensitive and recyclable SERS substrate based on Ag-nanoparticle-decorated ZnO nanoflowers in ordered arrays. *Dalton Trans.* **2015**, *44*, 3447−3453.

(92) Taylor, A. B.; Siddiquee, A. M.; Chon, J. W. M. Below melting point photothermal reshaping of single gold nanorods driven by surface diffusion. *ACS Nano* **2014**, *8* (12), 12071−12079.

(93) Tang, L.; Li, S.; Han, F.; Liu, L.; Xu, L.; Ma, W.; Kuang, H.; Li, A.; Wang, L.; Xu, C. SERS-active Au@Ag nanorod dimers for ultrasensitive dopamine detection. *Biosens. Bioelectron.* **2015**, *71*, 7−12.

(94) Zhang, L.-F.; Zhong, S.-L.; Xu, A.-W. Highly branched concave Au/Pd bimetallic nanocrystals with superior electrocatalytic activity and highly efficient SERS enhancement. *Angew. Chem. Int. Ed.* **2013**, *52* (2), 645−649.

(95) Zhang, C.; Jiang, S. Z.; Yang, C.; Li, C. H.; Huo, Y. Y.; Liu, X. Y.; Liu, A. H.; Wei, Q.; Gao, S. S.; Gao, X. G.; et al. Gold@silver bimetal nanoparticles/pyramidal silicon 3D substrate with high reproducibility for high-performance SERS. *Sci. Rep.* **2016**, *6*, 25243.

(96) Shen, J.; Su, J.; Yan, J.; Zhao, B.; Wang, D.; Wang, S.; Li, K.; Liu, M.; He, Y.; Mathur, S.; et al. Bimetallic nano-mushrooms with DNA-mediated interior nanogaps for high-efficiency SERS signal amplification. *Nano Res.* **2015**, *8* (3), 731−742.

(97) Khaywah, M. Y.; Jradi, S.; Louarn, G.; Lacroute, Y.; Toufaily, J.; Hamieh, T.; Adam, P. M. Ultrastable, uniform, reproducible, and highly sensitive bimetallic nanoparticles as reliable large scale SERS substrates. *J. Phys. Chem. C* **2015**, *119* (46), 26091−26100.

(98) Rao, V. K.; Radhakrishnan, T. P. Tuning the SERS response with Ag-Au nanoparticle-embedded polymer thin film substrates. *ACS Appl. Mater. Interfaces* **2015**, *7*, 12767−12773.

(99) Albe, K.; Klein, A. Density-functional-theory calculations of electronic band structure of single-crystal and single-layer WS_2. *Phys. Rev. B* **2002**, *66*, 073413.

(100) Mak, K. F.; Lee, C.; Hone, J.; Shan, J.; Heinz, T. F. Atomically Thin MoS_2: A New Direct-Gap Semiconductor. *Phys. Rev. Lett.* **2010**, *105*, 136805.

(101) Ding, Y.; Wang, Y.; Ni, J.; Shi, L.; Shi, S.; Tang, W. First principles study of structural, vibrational and electronic properties of graphene-like MX(2) (M = Mo, Nb, W, Ta; X = S, Se, Te) monolayers. *Phys. B* **2011**, *406*, 2254−2260.

(102) Ma, Y.; Dai, Y.; Guo, M.; Niu, C.; Lu, J.; Huang, B. Electronic and magnetic properties of perfect, vacancy-doped, and nonmetal adsorbed MoSe(2), MoTe(2) and WS(2) monolayers. *Phys. Chem. Chem. Phys.* **2011**, *13*, 15546−15553.

(103) Zhang, Y.; Chang, T. R.; Zhou, B.; Cui, Y. T.; Yan, H.; Liu, Z.; Schmitt, F.; Lee, J.; Moore, R.; Chen, Y.; et al. Direct observation of the transition from indirect to direct bandgap in atomically thin epitaxial $MoSe_2$. *Nat. Nanotechnol.* **2014**, *9*, 111−115.

(104) Muehlethaler, C.; Considine, C. R.; Menon, V.; Lin, W. C.; Lee, Y. H.; Lombardi, J. R. Ultrahigh Raman enhancement on monolayer MoS_2. *ACS Photonics* **2016**, *3*, 1164−1169.

(105) Lee, Y.; Kim, H.; Lee, J.; Yu, S. H.; Hwang, E.; Lee, C.; Ahn, J.-H.; Cho, J. H. Enhanced Raman Scattering of Rhodamine 6G Films on Two-Dimensional Transition Metal Dichalcogenides Correlated to Photoinduced Charge Transfer. *Chem. Mater.* **2016**, *28* (1), 180−187.

(106) Meng, L.; Hu, S.; Xu, C.; Wang, X.; Li, H.; Yan, X. Surface enhanced Raman effect on CVD growth of WS_2 film. *Chem. Phys. Lett.* **2018**, *707*, 71−74.

(107) Zhao, W.; Ghorannevis, Z.; Chu, L.; Toh, M.; Kloc, C.; Tan, P.-H.; Eda, G. Evolution of Electronic Structure in Atomically Thin Sheets of WS_2 and WSe_2. *ACS Nano* **2013**, *7* (1), 791−797.

(108) (a) Ling, X.; Wu, J.; Xu, W.; Zhang, J. Probing the Effect of Molecular Orientation on the Intensity of Chemical Enhancement Using Graphene Enhanced Raman Spectroscopy. *Small* **2012**, *8* (9), 1365−1372. (b) Yang, H.; Hu, H.; Ni, Z.; Poh, C. K.; Cong, C.; Lin, J.; Yu, T. Comparison of surface-enhanced Raman scattering on graphene oxide, reduced graphene oxide and graphene surfaces. *Carbon* **2013**, *62*, 422−429.

(109) Etchegoin, P. G.; Lacharmoise, P. D.; Le Ru, E. C. Influence of Photostability on Single-Molecule Surface Enhanced Raman Scattering Enhancement Factors. *Anal. Chem.* **2009**, *81* (2), 682−688.

(110) Zhao, Y.; Xie, Y.; Bao, Z.; Tsang, Y. H.; Xie, L.; Chai, Y. Enhanced SERS Stability of R6G Molecules with Monolayer Graphene. *J. Phys. Chem. C* **2014**, *118* (22), 11827−11832.

(111) Weng, J.; Zhao, S.; Li, Z.; Ricardo, K. B.; Zhou, F.; Kim, H.; Liu, H. Raman Enhancement and Photo-Bleaching of Organic Dyes in the Presence of Chemical Vapor Deposition-Grown Graphene. *Nanomaterials* **2017**, *7*, 337.

(112) Qiu, H.; Li, Z.; Gao, S.; Chen, P.; Zhang, C.; Jiang, S.; Xu, S.; Yang, C.; Li, H. Large-area MoS_2 thin layers directly synthesized on Pyramid-Si substrate for surface-enhanced Raman scattering. *RSC Adv.* **2015**, *5*, 83899−83905.

(113) Song, X.; Wang, Y.; Zhao, F.; Li, Q.; Ta, H. Q.; Rümmeli, M. H.; Tully, C. G.; Li, Z.; Yin, W.-J.; Yang, L.; Lee, K.-B.; Yang, J.; Bozkurt, I.; Liu, S.; Zhang, W.; Chhowalla, M. Plasmon-Free Surface-Enhanced Raman Spectroscopy Using Metallic 2D Materials. *ACS Nano* **2019**, *13* (7), 8312−8319.

(114) Lei, Z.; Wu, D.; Cao, X.; Zhang, X.; Tao, L.; Zheng, Z.; Feng, X.; Tao, L.; Zhao, Y. 2D platinum telluride as SERS substrate: Unique layer-dependent Raman enhanced effect. *J. Alloys Compd.* **2023**, *937*, 168294.

(115) Fraser, J. P.; Postnikov, P.; Miliutina, E.; Kolska, Z.; Valiev, R.; Švorčík, V.; Lyutakov, O.; Ganin, A. Y.; Guselnikova, O. Application of a 2D Molybdenum Telluride in SERS Detection of Biorelevant Molecules. *ACS Appl. Mater. Interfaces* **2020**, *12*, 47774−47783.

(116) Miao, P.; Qin, J.-K.; Shen, Y.; Su, H.; Dai, J.; Song, B.; Du, Y.; Sun, M.; Zhang, W.; Wang, H.-L.; Xu, C.-Y.; Xu, P. Unraveling the Raman Enhancement Mechanism on 1T′-Phase ReS_2 Nanosheets. *Small* **2018**, *14* (14), 1704079.

(117) Zhang, X.; Zou, J.; Zhang, X.; Wei, A.; luo, N.; Liu, Z.; Xu, J.; Zhao, Y. Controllable growth of 2D ReS_2 flakes and their surface Raman enhancement effects. *J. Alloys Compd.* **2023**, *963*, 171207.

(118) Wang, L.; Yu, D.; Huang, B.; Ou, Z.; Tao, L.; Tao, L.; Zheng, Z.; Liu, J.; Yang, Y.; Wei, A.; Zhao, Y. Large-area ReS_2 monolayer films on flexible substrate for SERS based molecular sensing with strong fluorescence quenching. *Appl. Surf. Sci.* **2021**, *542*, 148757.

(119) Tao, L.; Chen, K.; Chen, Z.; Cong, C.; Qiu, C.; Chen, J.; Wang, X.; Chen, H.; Yu, T.; Xie, W.; Deng, S.; Xu, J.-B. 1T′ Transition Metal Telluride Atomic Layers for Plasmon-Free SERS at Femtomolar Levels. *J. Am. Chem. Soc.* **2018**, *140* (28), 8696−8704.

(120) Su, S.; Zhang, C.; Yuwen, L.; Chao, J.; Zuo, X.; Liu, X.; Song, C.; Fan, C.; Wang, L. Creating SERS hot spots on MoS_2 nanosheets with in situ grown gold nanoparticles. *ACS Appl. Mater. Interfaces* **2014**, *6*, 18735−18741.
(121) Daeneke, T.; Carey, B. J.; Chrimes, A. F.; Ou, J. Z.; Lau, D. W. M.; Gibson, B. C.; Bhaskaran, M.; Kalantar-zadeh, K. Light driven growth of silver nanoplatelets on 2D MoS_2 nanosheet templates. *J. Mater. Chem. C* **2015**, *3*, 4771−4778.
(122) Zuo, P.; Jiang, L.; Li, X.; Li, B.; Ran, P.; Li, X.; Qu, L.; Lu, Y. Metal (Ag, Pt)−MoS_2 Hybrids Greenly Prepared Through Photochemical Reduction of Femtosecond Laser Pulses for SERS and HER. *ACS Sustainable Chem. Eng.* **2018**, *6* (6), 7704−7714.
(123) Lu, J. P.; Lu, J. H.; Liu, H. W.; Liu, B.; Gong, L.; Tok, E. S.; Loh, K. P.; Sow, C. H. Microlandscaping of Au nanoparticles on few-layer MoS2 films for chemical sensing. *Small* **2015**, *11*, 1792−1800.
(124) Zuo, P.; Jiang, L.; Li, X.; Li, B.; Xu, Y.; Shi, X.; Ran, P.; Ma, T.; Li, D.; Qu, L.; Lu, Y.; et al. Shape-Controllable Gold Nanoparticle−MoS_2 Hybrids Prepared by Tuning Edge-Active Sites and Surface Structures of MoS_2 via Temporally Shaped Femtosecond Pulses. *ACS Appl. Mater. Interfaces* **2017**, *9* (8), 7447−7455.
(125) Zhou, L.; Zhang, H.; Bao, H.; Liu, G.; Li, Y.; Cai, W. Decoration of Au Nanoparticles on MoS_2 Nanospheres: From Janus to Core/Shell Structure. *J. Phys. Chem. C* **2018**, *122* (15), 8628−8636.
(126) Kaushik, A.; Singh, J.; Soni, R.; Singh, J. P. MoS_2−Ag Nanocomposite-Based SERS Substrates with an Ultralow Detection Limit. *ACS Appl. Nano Mater.* **2023**, *6* (11), 9236−9246.
(127) Ghopry, S. A.; Sadeghi, S. M.; Berrie, C. L.; Wu, J. Z. MoS_2 Nanodonuts for High-Sensitivity Surface-Enhanced Raman Spectroscopy. *Biosensors* **2021**, *11*, 477.
(128) Sow, B. M.; Lu, J.; Liu, H.; Goh, K. E. J.; Sow, C. H. Sow, Enriched fluorescence emission from WS_2 monoflake empowered by Au nanoexplorers. *Adv. Optical Mater.* **2017**, *5*, 1700156.
(129) Mukherjee, B.; Sun Leong, W.; Li, Y.; Gong, H.; Sun, L.; Xiang Shen, Z.; Simsek, E.; Thong, J. T. L. Raman analysis of gold on WSe2 single crystal film. *Mater. Res. Exp.* **2015**, *2* (6), 065009.
(130) Abid, I.; Chen, W.; Yuan, J.; Najmaei, S.; Peñafiel, E. C.; Péchou, R.; Large, N.; Lou, J.; Mlayah, A. Surface enhanced resonant Raman scattering in hybrid MoSe2@Au nanostructures. *Opt. Express* **2018**, *26* (22), 29411−29423.
(131) Li, Y.; Liao, H.; Wu, S.; Weng, X.; Wang, Y.; Liu, L.; Qu, J.; Song, J.; Ye, S.; Yu, X.; Chen, Y. ReS_2 Nanoflowers-Assisted Confined Growth of Gold Nanoparticles for Ultrasensitive and Reliable SERS Sensing. *Molecules* **2023**, *28* (11), 4288.
(132) Jung, H. S.; Koh, E. H.; Mun, C.; Min, J.; Sohng, W.; Chung, H.; Yang, J.-Y.; Lee, S.; Kim, H. J.; Park, S.-G.; Lee, M.-Y.; Kim, D.-H. Hydrophobic hBN-coated surface-enhanced Raman scattering sponge sensor for simultaneous separation and detection of organic pollutants. *J. Mater. Chem. C* **2019**, *7*, 13059−13069.
(133) Jiang, S.; Guo, J.; Zhang, C.; Li, C.; Wang, M.; Li, Z.; Gao, S.; Chen, P.; Si, H.; Xu, S. A sensitive, uniform, reproducible and stable SERS substrate has been presented based on MoS_2@Ag nanoparticles@pyramidal silicon. *RSC Adv.* **2017**, *7*, 5764−5773.
(134) Tegegne, W. A.; Su, W.-N.; Tsai, M.-C.; Beyene, A. B.; Hwang, B.-J. Ag nanocubes decorated 1T-MoS_2 nanosheets SERS substrate for reliable and ultrasensitive detection of pesticides. *Appl. Mater. Today* **2020**, *21*, 100871.
(135) O'Hern, S. C.; Boutilier, M. S. H.; Idrobo, J. C.; Song, Y.; Kong, J.; Laoui, T.; Atieh, M.; Karnik, R. Selective ionic transport through tunable subnanometer pores in single-layer graphene membranes. *Nano Lett.* **2014**, *14*, 1234−1241.
(136) Suzuki, S.; Yoshimura, M. Chemical Stability of Graphene Coated Silver Substrates for Surface-Enhanced Raman Scattering. *Sci. Rep.* **2017**, *7*, 14851.
(137) Chen, P. X.; Qiu, H. W.; Xu, S. C.; Liu, X. Y.; Li, Z.; Hu, L. T.; Li, C. H.; Guo, J.; Jiang, S. Z.; Huo, Y. Y. A novel surface-enhanced Raman spectroscopy substrate based on a large area of MoS_2 and Ag nanoparticles hybrid system. *Appl. Surf. Sci.* **2016**, *375*, 207−214.
(138) Zheng, Z.; Cong, S.; Gong, W.; Xuan, J.; Li, G.; Lu, W.; Geng, F.; Zhao, Z. Semiconductor SERS enhancement enabled by oxygen incorporation. *Nat. Commun.* **2017**, *8*, 1993.
(139) Zuo, P.; Jiang, L.; Li, X.; Ran, P.; Li, B.; Song, A.; Tian, M.; Ma, T.; Guo, B.; Qu, L.; Lu, Y. Enhancing charge transfer with foreign molecules through femtosecond laser induced MoS_2 defect sites for photoluminescence control and SERS enhancement. *Nanoscale* **2019**, *11*, 485−494.
(140) Quan, Y.; Tang, X.-H.; Shen, W.; Li, P.; Yang, M.; Huang, X.-J.; Liu, W.-Q. Sulfur Vacancies-Triggered High SERS Activity of Molybdenum Disulfide for Ultrasensitive Detection of Trace Diclofenac. *Adv. Opt. Mater.* **2022**, *10* (23), 2201395.
(141) Jena, T.; Hossain, M. T.; Nath, U.; Sarma, M.; Sugimoto, H.; Fujii, M.; Giri, P. K. Evidence for intrinsic defects and nanopores as hotspots in 2D $PdSe_2$ dendrites for plasmon-free SERS substrate with a high enhancement factor. *npj 2D Mater. Appl.* **2023**, *7*, 8.
(142) Su, R.; Yang, S.; Han, D.; Hu, M.; Liu, Y.; Yang, J.; Gao, M. Ni and O co-modified MoS_2 as universal SERS substrate for the detection of different kinds of substances. *J. Colloid Interface Sci.* **2023**, *635*, 1−11.
(143) Jiang, L.; Xiong, S.; Yang, S.; Han, D.; Liu, Y.; Yang, J.; Gao, M. Neodymium doping MoS_2 nanostructures with remarkable surface-enhanced Raman scattering activity. *Ceram. Int.* **2023**, *49* (11), 19328−19337.
(144) Koklioti, M. A.; Bittencourt, C.; Noirfalise, X.; Saucedo-Orozco, I.; Quintana, M.; Tagmatarchis, N. Nitrogen-Doped Silver-Nanoparticle-Decorated Transition-Metal Dichalcogenides as Surface-Enhanced Raman Scattering Substrates for Sensing Polycyclic Aromatic Hydrocarbons. *ACS Appl. Nano Mater.* **2018**, *1* (7), 3625−3635.
(145) Tian, Y.; Wei, H.; Xu, Y.; Sun, Q.; Man, B.; Liu, M. Influence of SERS Activity of $SnSe_2$ Nanosheets Doped with Sulfur. *Nanomaterials* **2020**, *10*, 1910.
(146) Seo, J.; Kim, Y.; Lee, J.; Son, E.; Jung, M.-H.; Kim, Y.-M.; Jeong, H. Y.; Lee, G.; Park, H. A single-atom vanadium-doped 2D semiconductor platform for attomolar-level molecular sensing. *J. Mater. Chem. A* **2022**, *10*, 13298−13304.
(147) Liu, Y.; Gao, Z.; Chen, M.; Tan, Y.; Chen, F. Enhanced Raman scattering of CuPc films on imperfect WSe_2 monolayer correlated to exciton and charge-transfer resonances. *Adv. Funct. Mater.* **2018**, *28*, 1805710.
(148) Li, X.; Guo, S.; Su, J.; Ren, X.; Fang, Z. Efficient Raman Enhancement in Molybdenum Disulfide by Tuning the Interlayer Spacing. *ACS Appl. Mater. Interfaces* **2020**, *12* (25), 28474−28483.
(149) Sun, L.; Hu, H.; Zhan, D.; Yan, J.; Liu, L.; Teguh, J. S.; Yeow, E. K. L.; Lee, P. S.; Shen, Z. Plasma modified MoS_2 nanoflakes for surface enhanced Raman scattering. *Small* **2014**, *10*, 1090−1095.
(150) Pan, C.; Song, J.; Sun, J.; Wang, Q.; Wang, F.; Tao, W.; Jiang, L. One-Step Fabrication Method of MoS2 for High-Performance Surface-Enhanced Raman Scattering. *J. Phys. Chem. C* **2021**, *125*, 24550−24556.
(151) Ma, Y.; Dai, Y.; Guo, M.; Niu, C.; Huang, B. Graphene adhesion on MoS_2 monolayer: An ab initio study. *Nanoscale* **2011**, *3*, 3883−3887.
(152) Ghopry, S. A.; Alamri, M. A.; Goul, R.; Sakidja, R.; Wu, J. Z. Extraordinary Sensitivity of Surface-Enhanced Raman Spectroscopy of Molecules on MoS_2 (WS_2) Nanodomes/Graphene van der Waals Heterostructure Substrates. *Adv. Optical Mater.* **2019**, *7*, 1801249.
(153) Tan, Y.; Ma, L.; Gao, Z.; Chen, M.; Chen, F. Two-dimensional heterostructure as a platform for surface-enhanced Raman scattering. *Nano Lett.* **2017**, *17*, 2621−2626.
(154) Wu, D.; Chen, J.; Ruan, Y.; Sun, K.; Zhang, K.; Xie, W.; Xie, F.; Zhao, X.; Wang, X. A novel sensitive and stable surface enhanced Raman scattering substrate based on a MoS_2 quantum dot/reduced graphene oxide hybrid system. *J. Mater. Chem. C* **2018**, *6*, 12547−12554.
(155) Qiu, H.; Wang, M.; Zhang, L.; Cao, M.; Ji, Y.; Kou, S.; Dou, J.; Sun, X.; Yang, Z. Wrinkled 2H-phase MoS_2 sheet decorated with graphene-microflowers for ultrasensitive molecular sensing by plasmon-free SERS enhancement. *Sens. Actuators, B* **2020**, *320*, 128445.
(156) Lv, Q.; Tan, J.; Wang, Z.; Gu, P.; Liu, H.; Yu, L.; Wei, Y.; Gan, L.; Liu, B.; Li, J.; et al. Ultrafast charge transfer in mixed-dimensional

WO3-x nanowire/WSe_2 heterostructures for attomolar-level molecular sensing. *Nat. Commun.* **2023**, *14* (1), 2717.
(157) Tan, L.; Yue, S.; Lou, Y.; Zhu, J.-J. Enhancing charge transfer in a $W_{18}O_{49}$/g-C_3N_4 heterostructure via band structure engineering for effective SERS detection and flexible substrate applications. *Analyst* **2024**, *149*, 180−187.
(158) Majumdar, D. Surface-enhanced Raman effect on MoS_2−WS_2 composite structures. *Appl. Phys. A: Mater. Sci. Process.* **2024**, *130*, 289.
(159) Chen, L.; Hou, H.-L.; Prato, M. Impact of the Interlayer Distance between Graphene and MoS_2 on Raman Enhancement. *Chem. Mater.* **2023**, *35* (13), 5032−5039.
(160) Gogotsi, Y.; Anasori, B. The Rise of MXenes. *ACS Nano* **2019**, *13* (8), 8491−8494.
(161) Naguib, M.; Kurtoglu, M.; Presser, V.; Lu, J.; Niu, J.; Heon, M.; Hultman, L.; Gogotsi, Y.; Barsoum, M. W. Two-Dimensional Nanocrystals Produced by Exfoliation of Ti_3AlC_2. *Adv. Mater.* **2011**, *23*, 4248−4253.
(162) Naguib, M.; Mashtalir, O.; Carle, J.; Presser, V.; Lu, J.; Hultman, L.; Gogotsi, Y.; Barsoum, M. W. Two-Dimensional Transition Metal Carbides. *ACS Nano* **2012**, *6* (2), 1322−1331.
(163) Sarycheva, A.; Makaryan, T.; Maleski, K.; Satheeshkumar, E.; Melikyan, A.; Minassian, H.; Yoshimura, M.; Gogotsi, Y. Two-Dimensional Titanium Carbide (MXene) as Surface-Enhanced Raman Scattering Substrate. *J. Phys. Chem. C* **2017**, *121* (36), 19983−19988.
(164) Shevchuk, K.; Sarycheva, A.; Gogotsi, Y. Evaluation of two-dimensional transition-metal carbides and carbonitrides (MXenes) for SERS substrates. *MRS Bull.* **2022**, *47*, 545−554.
(165) Limbu, T. B.; Chitara, B.; Garcia Cervantes, M. Y.; Zhou, Y.; Huang, S. Y.; Tang, Y.; Yan, F. Unravelling the Thickness Dependence and Mechanism of Surface-Enhanced Raman Scattering on $Ti_3C_2T_X$ MXene Nanosheets. *J. Phys. Chem. C* **2020**, *124* (32), 17772−17782.
(166) Liu, R.; Jiang, L.; Lu, C.; Yu, Z.; Li, F.; Jing, X.; Xu, R.; Zhou, W.; Jin, S. Large-scale two-dimensional titanium carbide MXene as SERS-active substrate for reliable and sensitive detection of organic pollutants. *Spectrochim. Acta, Part A* **2020**, *236*, 118336.
(167) Soundiraraju, B.; George, B. K. Two-dimensional titanium nitride (Ti_2N) MXene: synthesis, characterization, and potential application as surface-enhanced Raman scattering substrate. *ACS Nano* **2017**, *11*, 8892−8900.
(168) He, Z.; Rong, T.; Li, Y.; Ma, J.; Li, Q.; Wu, F.; Wang, Y.; Wang, F. Two-Dimensional TiVC Solid-Solution MXene as Surface-Enhanced Raman Scattering Substrate. *ACS Nano* **2022**, *16* (3), 4072−4083.
(169) Satheeshkumar, E.; Makaryan, T.; Melikyan, A.; Minassian, H.; Gogotsi, Y.; Yoshimura, M. One-step Solution Processing of Ag, Au and Pd@MXene Hybrids for SERS. *Sci. Rep.* **2016**, *6*, 32049.
(170) Wang, T.; Dong, P.; Zhu, C.; Gao, W.; Sha, P.; Wu, Y.; Wu, X. Fabrication of 2D titanium carbide MXene/Au nanorods as a nanosensor platform for sensitive SERS detection. *Ceram. Int.* **2021**, *47*, 30082−30090.
(171) Xie, H.; Li, P.; Shao, J.; Huang, H.; Chen, Y.; Jiang, Z.; Chu, P. K.; Yu, X.-F. Electrostatic Self-Assembly of $Ti_3C_2T_x$ MXene and Gold Nanorods as an Efficient Surface-Enhanced Raman Scattering Platform for Reliable and High-Sensitivity Determination of Organic Pollutants. *ACS Sens.* **2019**, *4* (9), 2303−2310.
(172) Yusoff, N. N.; Nor Azmi, F. S.; Abu Bakar, N.; Tengku Abdul Aziz, T. H.; Shapter, J. G. Titanium carbide MXene/silver nanostars composite as SERS substrate for thiram pesticide detection. *Chem. Pap.* **2024**, *78*, 2855−2865.
(173) Bai, Y.; Otitoju, T. A.; Wang, Y.; Chen, Q.; Sun, T. Highly sensitive in situ SERS monitoring of Fenton-like reaction by a PDDA-MXene@AuNP composite. *New J. Chem.* **2023**, *47*, 5174−5178.
(174) Peng, Y.; Cai, P.; Yang, L.; Liu, Y.; Zhu, L.; Zhang, Q.; Liu, J.; Huang, Z.; Yang, Y. Theoretical and Experimental Studies of Ti_3C_2 MXene for Surface-Enhanced Raman Spectroscopy-Based Sensing. *ACS Omega* **2020**, *5*, 26486−26496.
(175) Wu, Z.; Sun, D.-W.; Pu, H.; Wei, Q.; Lin, X. $Ti_3C_2T_x$ MXenes loaded with Au nanoparticle dimers as a surface-enhanced Raman scattering aptasensor for AFB1 detection. *Food Chem.* **2022**, *372*, 131293.
(176) Chen, Y.; Jiang, C.; Huang, F.; Yu, Z.; Jiang, L. Efficient interfacial self-assembled MXene/Ag NPs film nanocarriers for SERS-traceable drug delivery. *Anal. Bioanal. Chem.* **2023**, *415*, 5379−5389.
(177) Yoo, S. S.; Ho, J.-W.; Shin, D.-I.; Kim, M.; Hong, S.; Lee, J. H.; Jeong, H. J.; Jeong, M. S.; Yi, G.-R.; Kwon, S. J.; Yoo, P. J. Simultaneously intensified plasmonic and charge transfer effects in surface enhanced Raman scattering sensors using an MXene-blanketed Au nanoparticle assembly. *J. Mater. Chem. A* **2022**, *10*, 2945−2956.
(178) Liu, X.; Dang, A.; Li, T.; Sun, Y.; Lee, T.-C.; Deng, W.; Wu, S.; Zada, A.; Zhao, T.; Li, H. Plasmonic Coupling of Au Nanoclusters on a Flexible MXene/Graphene Oxide Fiber for Ultrasensitive SERS Sensing. *ACS Sens.* **2023**, *8* (3), 1287−1298.
(179) Limbu, T. B.; Chitara, B.; Orlando, J. D.; Garcia Cervantes, M. Y.; Kumari, S.; Li, Q.; Tang, Y.; Yan, F. Green synthesis of reduced $Ti_3C_2T_x$ MXene nanosheets with enhanced conductivity, oxidation stability, and SERS activity. *J. Mater. Chem. C* **2020**, *8*, 4722−4731.
(180) Lombardi, J. R.; Birke, R. L. Theory of surface-enhanced Raman scattering in semiconductors. *J. Phys. Chem. C* **2014**, *118*, 11120−11130.
(181) Kim, J.; Jang, Y.; Kim, N.-J.; Kim, H.; Yi, G.-C.; Shin, Y.; Kim, M. H.; Yoon, S. Study of Chemical Enhancement Mechanism in Non-plasmonic Surface Enhanced Raman Spectroscopy (SERS). *Front. Chem.* **2019**, *7*, 582.
(182) Kim, N.-J.; Kim, J.; Park, J.-B.; Kim, H.; Yi, G.-C.; Yoon, S. Direct observation of quantum tunnelling charge transfers between molecules and semiconductors for SERS. *Nanoscale* **2019**, *11*, 45−49.
(183) Jia, S.; Bandyopadhyay, A.; Kumar, H.; Zhang, J.; Wang, W.; Zhai, T.; Shenoy, V. B.; Lou, J. Biomolecular sensing by surface-enhanced Raman scattering of monolayer Janus transition metal dichalcogenide. *Nanoscale* **2020**, *12*, 10723−10729.